

# Boosting the dark matter signal with Coulomb resonances

Rakhi Mahbubani<sup>a,b</sup> and Kin Mimouni<sup>a</sup>

<sup>a</sup>Theoretical Particle Physics Laboratory (LTP), Institute of Physics, EPFL, Lausanne, Switzerland.

<sup>b</sup>Albert Einstein Center for Fundamental Physics, Institute for Theoretical Physics, University of Bern, Sidlerstrasse 5, CH-3012 Bern, Switzerland

E-mail: [rakhi@cern.ch](mailto:rakhi@cern.ch), [kin.mimouni@epfl.ch](mailto:kin.mimouni@epfl.ch)

**Abstract.** We show that the presence of nearby Coulombic resonances at finite energy could lead to the enhancement of the dark matter annihilation cross section at specific non-zero velocities correlated with the mass splitting between the dark matter pair and that of the resonance. If one of these resonant velocities approximately matches the velocity of dark matter in our local neighbourhood, we would see this enhancement in existing indirect-detection measurements, such as the measurements of the continuum photon spectrum made by HESS and Fermi-LAT. We explore this effect in the context of pure Higgsino and Wino dark matter with a variable splitting between charged and neutral components, controlled by the Wilson coefficient of a higher-dimension operator. For electroweak WIMPs a relevant and appreciable enhancement from Coulomb resonances requires tuning the charged-neutral splitting to be of order the Coulomb binding energies. This leads to strong exclusions of Higgsino dark matter with charged-neutral splittings in the narrow ranges (2, 2.5) and (8.5, 10.5) MeV. In contrast, by decreasing the charged-neutral splitting for the thermal Wino, we can move the Yukawa resonance away from the thermal relic mass, decreasing the indirect-detection signal to a level that is compatible with HESS measurements in the window (25, 35) MeV.

---

## Contents

<b>1 Sommerfeld enhancement</b>	<b>2</b>
1.1 Some analytical considerations	5
<b>2 Simplified electroweak models</b>	<b>7</b>
2.1 Electroweak Sommerfeld factors	9
<b>3 Indirect detection</b>	<b>12</b>
<b>4 Two complete models</b>	<b>16</b>
4.1 MSSM	16
4.2 Dirac gaugino	19
<b>5 Conclusion</b>	<b>20</b>
<b>A Annihilation matrices</b>	<b>22</b>
<b>B Relic density calculation</b>	<b>24</b>
B.1 Pure Higgsino	25
B.2 Pure Wino	26

---

## Introduction

There is compelling astrophysical and cosmological evidence for the existence of Dark Matter (DM) that calls for physics beyond the Standard Model (SM). The simplest solution is the Weakly-Interacting Massive Particle (WIMP) paradigm. This consists of a new weakly-interacting state whose interaction with the SM freezes out of thermal equilibrium, naturally yielding the measured dark matter density for mass around a TeV, the scale by which we also already expected to have seen the New Physics that solved the hierarchy problem. The slow erosion of the latter hope by null results at the LHC has devalued the currency of the WIMP paradigm, opening up the parameter space for viable dark matter to both extremely light and extremely heavy scales, and resulting in a frenzy of theoretical and experimental activity at the boundary of condensed matter and astroparticle physics (see e.g. [1] and references therein). Nevertheless the original WIMP solution lives on - its small cross section making it hard to probe at hadron colliders, particularly for a fairly pure Higgsino with loop-induced splittings, and greater ingenuity [2, 3] (or perhaps future colliders [4, 5]) will be required to discover or exclude it.

A large separation of scales between the mass of the dark matter particle and that of its force carriers, could lead to a non-perturbative enhancement of its annihilation cross section in the nonrelativistic limit due to multi- gauge boson exchange. This Sommerfeld enhancement, first documented in the context of multi-photon exchange by electrons [6], was later demonstrated [7, 8] to affect the mass and indirect detection cross section of a pure Wino thermal relic. The significant enhancement of the latter can be seen as due to the accidental presence of a ‘zero-energy’ resonance close to the DM-DM ground state at the relic mass, loosely bound by the attractive Yukawa potential between the neutral particles

[7]. This is not the case for the Higgsino relic, the Yukawa potential having no bound state for DM mass around the relic mass.

In addition to a potential global enhancement at low velocity due to zero-energy bound states of dark matter, there can also be a significant enhancement of the dark matter annihilation cross section at *specific* velocities due to quasi-bound states of a nearby, more massive two-particle state. For simplicity, in this work we will illustrate this behaviour using pure Higgsino and pure Wino dark matter as simple test cases. In these examples electroweak loop corrections lift the mass of the charged component with respect to the neutral one by  $\delta m \sim \alpha m_Z$ , and gauge boson exchange allows mixing between the neutral-neutral ( $\text{DM}^0\text{DM}^0$ ) and heavier charged-charged ( $\text{DM}^+\text{DM}^-$ ) two-particle states. The dark matter spectrum will also contain various two-particle states that are loosely bound by the long-range interactions. The lowest-lying state will be the  $\text{DM}^0\text{DM}^0$  quasi-bound state responsible for the large boost in the Wino annihilation cross-section. More central to our argument, however, is the tower of Coulomb  $\text{DM}^+\text{DM}^-$  resonances that lie between the free  $\text{DM}^0\text{DM}^0$  and  $\text{DM}^+\text{DM}^-$  two-particle states. When the incoming dark matter particles have just enough energy to create these states, their annihilation cross section is resonantly enhanced; this enhancement only occurs for certain specific values of the incoming velocity that match the mass difference between the ground state and the resonance.

For pure Wino/Higgsino states with nominal splitting, the Coulomb binding energies  $E_{B,\gamma} = \alpha^2 M_\chi / (4n^2)$  are negligible compared with the splittings, so the resonant velocities ( $\beta \sim 10^{-2}$ ) are irrelevant for any measured physical processes. Nevertheless in any scenario where the Coulomb binding energy is of the order of the splitting, the lowest-lying resonances could be brought close enough to the ground state to give a large boost to the indirect-detection signal for dark matter at velocities relevant to existing measurements in our galactic centre (GC) and/or nearby dwarf spheroidal galaxies (DSG). Hence varying the charged-neutral splitting, via a higher-dimension operator originating from integrating out heavy new physics for example, could give rise to significant changes in the cosmology and phenomenology of the dark matter candidate by tuning Yukawa and Coulomb resonances in and out of relevant regions of phase space.

We begin this work with a review of Sommerfeld enhancement in Section 1, building some intuition for this phenomenon using simple scenarios where it can be computed analytically. We continue in Section 2 with an exposition of our simplified model framework, consisting of the SM with the addition of a weak-doublet (triplet) fermion with hypercharge 1/2 (0) and Dirac (Majorana) mass, corresponding to the pure Higgsino (Wino) limit of the Minimal Supersymmetric Standard Model (MSSM). We assume that the charged-neutral splitting is a free parameter, varied using the Wilson coefficient of a higher-dimension operator. We consider the effect of varying the splitting on the indirect-detection cross section in Section 3, focussing on the continuum photon spectrum which does not suffer from the large propagation uncertainties of hadronic final states. We compare the results with existing measurements from HESS and Fermi-LAT. Finally we set our simplified model within the context of the MSSM, and the MSSM with Dirac gauginos in Section 4. We present our conclusions and outlook in Section 5.

## 1 Sommerfeld enhancement

This is the enhancement of the short-distance cross section for a process due to the distortion of the wave function for the incoming state by a long-range potential. This effect increases

with decreasing velocity, and was first noticed by Sommerfeld [6] in the context of electromagnetism. It has a classical gravitational analogue in the low-velocity enhancement of the cross section for a point particle hitting a massive object of radius  $R$  [9]:

$$\sigma = \pi R^2 \left( 1 + \frac{\beta_{\text{esc}}^2}{\beta^2} \right) \quad (1.1)$$

where  $\beta$  is the velocity of the point particle and  $\beta_{\text{esc}} = 2G_N M/R$  is the escape velocity from the surface of the extended object.

In quantum field theory it can be seen as the enhancement due to ladder diagrams in which a light force-carrier is exchanged. For non-relativistic muon annihilation for example, the amplitude for the  $n^{\text{th}}$ -order ladder diagram (due to  $n$  photon exchanges between the muon pair) is proportional to  $(\alpha/\beta)^n$  in the non-relativistic limit, which means the perturbative expansion in  $\alpha$  breaks down for small enough velocity, and the ladder diagrams must be systematically resummed. As shown in [8] the Sommerfeld factor can be determined by factorizing the short-distance and long-distance behaviour. The distorting effect of the long-range potential  $V(r)$  on the two-particle wavefunction is computed by solving the Schrödinger equation in the presence of only this potential, and the total enhancement then computed by perturbing around the resulting inhomogeneous solution at leading order in the absorptive part, which encodes the short-distance behaviour. The same procedure was proved in [10] to be equivalent to explicit resummation of the ladder diagrams.

Two particles subject to a long-range potential  $V(|\vec{r}|)$ , satisfy the following Schrödinger equation in the centre-of-mass frame, where  $\psi(\vec{r})$  is the two-particle wavefunction:

$$-\frac{1}{2\mu} \nabla^2 \psi(\vec{r}) + V(|\vec{r}|) \psi(\vec{r}) = \frac{1}{2} \mu \dot{\vec{r}}^2 \psi(\vec{r}) \quad (1.2)$$

with  $\mu$  is the reduced mass of the system.

Separating variables to isolate the radial and angular parts as usual, we obtain, for two particles of equal mass  $m_1 = m_2 = M$ , with velocity  $\beta$  in the centre-of-mass frame<sup>1</sup>, the following radial equation:

$$-\frac{1}{M} \frac{1}{r^2} \frac{d}{dr} \left( r^2 \frac{dR}{dr} \right) + \left( \frac{l(l+1)}{Mr^2} + V(r) - M\beta^2 \right) R = 0 \quad (1.3)$$

To isolate the dominant ( $s$ -wave) contribution, we take  $l = 0$ ; substituting  $R(r) = \chi(r)/r$  we obtain

$$\chi''(r) + (M^2\beta^2 - M V(r)) \chi(r) = 0. \quad (1.4)$$

This equation cannot be solved analytically for general potentials  $V(r)$ , but we can solve numerically for the irregular solution, which satisfies the boundary conditions:

$$\chi(0) = 1, \chi'(\infty) = -iM\beta\chi(\infty) \quad (1.5)$$

and then compute the Sommerfeld-enhanced cross section as

$$\sigma \equiv S \sigma_0 = \frac{|\chi(\infty)|^2}{|\chi(0)|^2} \sigma_0 \quad (1.6)$$

---

<sup>1</sup>We use the velocity  $\beta$  such that in the non-relativistic limit we have the Mandelstam variable  $s = 4M^2 + 4M^2\beta^2 + O(\beta^4)$

where  $\sigma_0$  is the perturbative cross-section and  $S$  denotes the Sommerfeld enhancement factor.<sup>2</sup>

This method can be generalized to the case where there is an interaction that mixes distinct two-particle states. For  $N$  two-particle states  $\chi_i(r)$ , with  $i = 1, \dots, N$ , the Sommerfeld enhancement can be computed by numerically solving the following set of  $N$  coupled radial Schrödinger equations:

$$\chi_i''(r) + M^2\beta^2\chi_i(r) - M \sum_j V_{ik}^{\text{tot}}(r)\chi_k(r) = 0 \quad (1.8)$$

$N$  times, with a different boundary condition at  $r = 0$  each time, representing each distinct two-particle state participating in the short-distance interaction:  $\chi_i(0)|_j = \delta_{ij}$  for the  $j^{\text{th}}$  solution. The boundary condition at infinity corresponds to a pure outgoing (decaying) wave for  $(M\beta^2 - V(r \rightarrow \infty))$  positive (negative). Here all energies/potentials are defined with respect to the lightest two-particle state, consisting of two identical particles of mass  $M$ . Any mass differences with respect to the lightest state show up as additional radius-independent contributions to the total potential.<sup>3</sup>

The cross-section in the  $i^{\text{th}}$  channel is then given by:

$$\sigma_i = c_i(A \cdot \Gamma \cdot A^\dagger)_{ii} \quad (1.9)$$

where  $\Gamma_{jk}$  is the absorptive part of the two-to-two cross section  $\chi_j \rightarrow \chi_k$ , with  $j, k$  running over all possible two-particle states in each channel.  $c_i$  is a numerical factor that accounts for the different normalization of the two-body wavefunctions for identical and non-identical particles:  $c_i = 2$  ( $c_i = 1$ ) when the two particles are identical (distinct). The matrix  $A$  is computed as:

$$A_{ij} = \lim_{r \rightarrow \infty} \frac{\chi_i(r)|_j}{e^{i\sqrt{M(M\beta^2 - V_{ii}(\infty))}r}}. \quad (1.10)$$

We can also define a Sommerfeld factor in each channel  $i$ , in analogy with the unmixed case:

$$S_i = c_i \frac{(A \cdot \Gamma \cdot A^\dagger)_{ii}}{\Gamma_{ii}}. \quad (1.11)$$

Note that unlike in the unmixed case the mixed Sommerfeld factor is not only dependent on the potential, but also on the  $\Gamma$  matrix for the hard process of interest.

In practice, for mixed channels we must solve for the Sommerfeld factor numerically. The numerical stability of the solution is an issue in the multi-state scenario, since the presence of an exponentially decaying part in the charged-charged wavefunction (due to the charged-neutral mass difference) makes the solution particularly unstable to rounding errors. Special care must be taken in the numerical recipe in order to favour convergence. We use the variable phase method, as detailed in [11].

---

<sup>2</sup>This procedure was shown in [9] to be equivalent to finding the regular solution and computing the enhancement using

$$S = \left| \frac{\frac{d\chi}{dr}(0)}{k} \right|^2 \quad (1.7)$$

<sup>3</sup>Note for states  $\chi_i$  with mass  $M + \delta m_i$ ,  $\beta$  is *not* the physical initial velocity of the particle, but is defined such that the total energy of the heavy-particle pair with respect to the dark-matter pair is  $E = M\beta^2$ . The Sommerfeld enhancement calculation takes into account that the state  $\chi_i$  cannot exist as an asymptotic state for  $M\beta^2 < \delta m_i$ .

## 1.1 Some analytical considerations

The electroweak potentials that we will consider have three individual constituents that combine in a complex way: the Coulomb interaction, the Yukawa interaction due to weak gauge boson exchange, and a mass splitting between different sets of asymptotic states. The effect on the Sommerfeld factor of each of these components individually can be understood analytically. Following [12], we will review these arguments below in order to build some intuition before we move on to tackle the full electroweak case in Section 2.1 below.

### Pure Coulomb potential

We first consider the scattering of a pair of particles of mass  $M$  and velocity  $\beta$  in their centre-of-mass frame interacting via a Coulomb potential  $V(r) = \pm\alpha/r$ , where the Sommerfeld factor can be computed analytically [9, 13]:

$$S = \left| \frac{\mp \frac{\pi\alpha}{\beta}}{1 - e^{\pm \frac{\pi\alpha}{\beta}}} \right|. \quad (1.12)$$

The enhancement is determined by the relative significance of the Coulomb binding energy  $\alpha^2 M$  of the incoming particles and their kinetic energy of,  $M\beta^2$ , and is large when the binding energy dominates. Hence the Sommerfeld factor is independent of the particle  $M$ , and grows with  $\alpha/\beta$  for an attractive potential, approaching unity for large velocities as expected (in practice the arbitrary growth at small  $\beta$  will be cut off by finite temperature effects, when the photon acquires a thermal mass). For a repulsive potential it gives rise to an exponential suppression, due to the presence of a Coulomb barrier:

$$\lim_{\beta \rightarrow 0} S \sim \begin{cases} \frac{\pi\alpha}{\beta} & \text{attractive } V \\ \frac{\pi\alpha}{\beta} e^{-\frac{\pi\alpha}{\beta}} & \text{repulsive } V \end{cases} \quad (1.13)$$

### Pure Yukawa potential

The enhancement due to a Yukawa potential  $V(r) = \pm\frac{\alpha}{r}e^{-M_V r}$ , arising from the exchange of a massive gauge boson of mass  $M_V$ , can only be treated analytically by approximating the Yukawa potential as a Hulthén potential:

$$V(r) = \pm\alpha \frac{kM_V e^{-kM_V r}}{1 - e^{-kM_V r}} \quad (1.14)$$

where  $k$  is a fudge factor chosen phenomenologically to match the short- and long-range behaviour of the Yukawa potential ( $k = \frac{\pi^2}{6}$  for  $s$ -wave enhancement [14]). The Sommerfeld factor can be expressed in closed form [12, 14, 15]:

$$S = \mp \frac{\pi\alpha}{\beta} \frac{\sinh\left(\frac{2\pi M}{kM_V}\beta\right)}{\cosh\left(\frac{2\pi M}{kM_V}\beta\right) - \cos\left(\frac{2\pi M}{kM_V}\beta\sqrt{\mp \frac{kM_V}{M} \frac{\alpha}{\beta^2} - 1}\right)} \quad (1.15)$$

The Yukawa form of the potential brings into play another relevant quantity: the size of the Bohr radius,  $(\alpha M)^{-1}$  relative to the range of the potential  $M_V^{-1}$ ; the Sommerfeld enhance-

ment grows with  $\alpha M/M_V$ :

$$\lim_{\beta \rightarrow 0} S \sim \begin{cases} 2k \left( \frac{\alpha}{\beta} \right)^2 \frac{M_V}{\alpha M} & \text{attractive } V, \ M = n^2 \frac{k M_V}{\alpha} \quad \text{for integer } n \\ \frac{2\pi^2}{k} \frac{\alpha M}{M_V} \left( 1 - \cos \left( 2\pi \sqrt{\frac{\alpha M}{k M_V}} \right) \right)^{-1} & \text{attractive } V, \text{ non-resonant } M \\ \frac{2\pi^2}{k} \frac{\alpha M}{M_V} \left( \cosh \left( 2\pi \sqrt{\frac{\alpha M}{k M_V}} \right) - 1 \right)^{-1} & \text{repulsive } V \end{cases} \quad (1.16)$$

Unlike that for the Coulomb potential, the Sommerfeld factor for an attractive Yukawa potential tends to a constant as  $\beta$  approaches zero, except for specific values of  $M$  where the denominator of (1.16) vanishes, and the Sommerfeld factor undergoes even faster growth, as  $1/\beta^2$ . These values of  $M$  correspond to instances where the Hulthén potential admits zero-energy bound states. For a repulsive Yukawa potential, the Sommerfeld factor again tends to a constant, that smaller than one, and there is no resonant structure.

For larger values of  $\beta$ , the hyperbolic functions simplify and  $S \sim \pi\alpha/\beta$  as in the electromagnetic case. The transition between the two regimes happens around  $\beta \sim M_V/M$  [9], where the de Broglie wavelength of the particle becomes of order the range of the Yukawa interaction, and the particle begins to probe the short-range nature of the potential. See Figure 1 for a graphical display of the behaviour of Sommerfeld factor for an attractive Yukawa potential as a function of  $\beta/\alpha$ , for  $M_V(\alpha M)^{-1} = 0.2$  (solid green curve), as compared with the growth for an on-resonance mass,  $M = M^* = kn^2 M_V/\alpha$  (solid yellow curve).

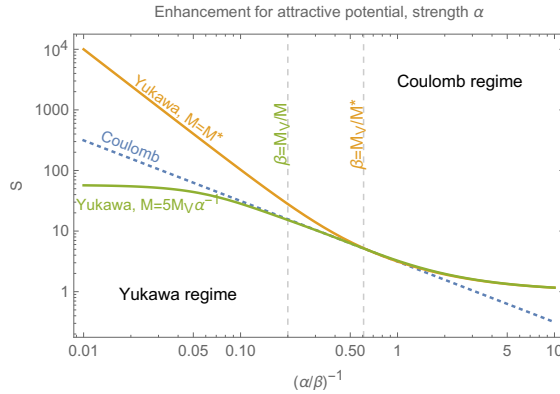


**Figure 1.** Sommerfeld enhancement for an attractive Yukawa potential, showing both off-resonance saturation for  $M_V(\alpha M)^{-1} = 1/5$  (solid green curve), and on-resonance growth for  $M = M^* = kn^2 M_V/\alpha$  (solid yellow curve). The enhancement for a pure Coulomb potential is shown for comparison (dashed blue line). For further explanation of symbols, see text.

## Mass splitting

The introduction of a mass splitting  $\delta m$  between the incoming state and a nearby state with which it mixes has two important consequences. Above some threshold velocity

$$\beta_{\text{th}} = \sqrt{2 \frac{\delta m}{M}}, \quad (1.17)$$

a pair of incoming states can scatter inelastically to a pair of heavy partners on-shell, giving the light states access to a new, perhaps stronger, annihilation channel. More crucial to our narrative, however, are the large enhancements that can occur at particular velocities below the heavy-particle threshold, due to threshold production of loosely-bound resonances of the heavy partner pair, lying between the light and heavy states in the mass spectrum. For a resonance with binding energy  $E_B$ , the corresponding resonant velocity can be written as:

$$\beta^* = \sqrt{\frac{2\delta m - E_B}{M}} \quad (1.18)$$

The physically-relevant parameter encoding the splitting is then  $\delta m/E_B$ . The enhancement due to these below-threshold resonances was observed in [12, 16, 17], but their possible effects on the phenomenology of dark matter were not explored.

### Mixed electroweak potential

We will be concerned with a two-component non-relativistic potential, due to mixing between the charged ( $\text{DM}^+\text{DM}^-$ ) and neutral ( $\text{DM}^0\text{DM}^0$ ) components of the dark matter multiplet, that takes the following schematic form:

$$V = \begin{pmatrix} \delta m + V_C + V_Y & V_Y \\ V_Y & V_Y \end{pmatrix} \quad (1.19)$$

where  $V_C$ ,  $V_Y$  denote the Coulomb and Yukawa potentials, with coupling strength scaling like  $\alpha$  and  $\alpha_L$ , respectively. The combined effect on the Sommerfeld factor will result in different behaviour in different velocity regimes, as follows:

- High  $\beta$ ,  $\beta \gg \frac{m_W}{M}$ ,  $\beta_{th}$ : in this regime we can neglect the mass splitting and trust the analytical expressions for the Sommerfeld factor. The Yukawa contribution is of order  $S_L \sim \pi\alpha_L/\beta$  and the electromagnetic contribution is of order  $S_{em} \sim \pi\alpha/\beta$  and since  $\alpha_L > \alpha$  we expect the Yukawa potential to dominate.
- Intermediate  $\beta$ ,  $\frac{m_W}{M} > \beta > \beta_{th}$ : in this regime we can also neglect the mass splitting. Off resonance, the Yukawa contribution goes to a constant of order  $S_L \sim \alpha_L M/m_W$  while the electromagnetic contribution continues to grow like  $S_{em} \sim \pi\alpha/\beta$ , so we expect the electromagnetic attraction to dominate. On resonance however, the Yukawa contribution behaves like  $1/\beta^2$  and is the dominant one.
- Low  $\beta$ ,  $\beta < \beta_{th}$ : the  $\delta m$  term in the potential dominates. In charged channels, the Sommerfeld factor is zero by construction because an initial on-shell charged pair cannot have an energy below  $2(M + \delta m)$ . Just below threshold the neutral channels exhibit resonant enhancement due to Coulomb resonances of  $\text{DM}^+\text{DM}^-$ . As  $\beta$  decreases still further, the weak Yukawa potential dominates.

We will see these different types of behaviour in the context of pure Higgsino and Wino simplified models in Section 2 below.

## 2 Simplified electroweak models

We will explore the Sommerfeld enhancement due to the partner resonances in the framework of two simplified models, corresponding to the pure Higgsino and pure Wino limits of the



MSSM, with the addition of the leading higher-dimension operators that affect the tree-level mass spectrum in each case. Our arguments will be placed within the context of the MSSM and the MSSM with Dirac gauginos in Section 2.

Our first example consists of the Standard Model with the addition of a vector-like  $SU(2)_L$  doublet  $\chi$  of fermions. In order to have an electrically-neutral thermal relic candidate,  $\chi$  must have hypercharge  $Y = \frac{1}{2}$  and thus be a Dirac doublet. The Lagrangian for  $\chi = (\chi^+, \chi^0)$  is:

$$\mathcal{L}_{\text{doublet}} = \mathcal{L}_{\text{SM}} + i\bar{\chi}\not{D}\chi - M\bar{\chi}\chi + c_1 H^\dagger H \bar{\chi}\chi + c_2 H^\dagger \frac{\sigma^a}{2} H \bar{\chi} \frac{\sigma^a}{2} \chi + \dots \quad (2.1)$$

where we have included the leading corrections to the dark matter mass due to new physics, in the form of dimension-5 operators with arbitrary Wilson coefficients  $c_1$  and  $c_2$ . If the new physics has coupling  $g_*$  and mass  $M_*$ , we would expect these coefficients to be  $\mathcal{O}(g_*^2/M_*^2)$ , up to an order-one constant.

We enforce stability of the DM candidate  $\chi^0$  by imposing a global symmetry that preserves DM number (in the MSSM it is  $R$ -parity), forbidding terms such as  $\bar{L}\chi$  in the Lagrangian (where  $L$  is the lepton doublet).

Setting the Higgs to its vacuum-expectation value (VEV), we immediately see that the first term is a global shift of the charged and neutral DM mass, which we can redefine away, whereas the second term gives rise to the following mass splitting between the states:

$$\delta m = M_{\chi^+} - M_{\chi^0} = \frac{c_2 v^2}{2} = \frac{c_2 m_W^2}{2g_L^2} \quad (2.2)$$

This splitting can be positive or negative, depending on the sign of  $c_2$ , and could be as large as 2 GeV for a new physics state of mass  $M_* \sim 4$  TeV with weak coupling  $g_* \sim 1$ . There is also a contribution to the splitting coming from electroweak loops. This is due to different wave-function renormalization for the neutral and charged state from a photon and  $Z$ -boson loop, and takes the form [18]:

$$\delta m = M_{\chi^+} - M_{\chi^0} = \frac{\alpha M}{2\pi} \int_0^1 dx (1+x) \log \left( 1 + \frac{1-x}{x^2} \frac{m_Z^2}{M^2} \right) \quad (2.3)$$

where  $M$  is the DM mass. In the limit we are interested in, namely  $M \gg m_Z$  this integral reduces to  $\delta m = \frac{\alpha m_Z}{2\pi} = 344$  MeV.

Because it has a non-zero hypercharge, the doublet has a direct coupling to the  $Z$  boson and a scattering cross-section on nuclei around  $10^{-39}$  cm<sup>2</sup>, several orders of magnitude larger than the limits imposed by direct detection experiments [19]. A way around this is to assume that the neutral state  $\chi^0$  has a mass mixing with a neutral Majorana state that splits the Dirac fermion into two Majorana fermions  $\chi_1$  and  $\chi_2$ . The lightest state  $\chi_1$  is the DM candidate and has no diagonal  $Z\chi_1\chi_1$  coupling. This scenario occurs naturally in the MSSM where the neutral Higgsino components mix with the Bino and neutral Wino. Then the direct detection process goes through the off-diagonal  $Z$ -coupling and is the inelastic reaction:  $\chi_1 N \rightarrow \chi_2 N$ . If  $M_{\chi_2} - M_{\chi_1} \geq 350$  keV or so (depending on the nucleus), this process is kinematically forbidden and cannot be seen in direct detection experiments [20]. In the remainder of this work we will be assuming that such a neutral splitting is present, and is large enough to avoid direct detection constraints, but has a negligible effect on our Sommerfeld calculations.

Our second simplified model consists of the SM lagrangian plus a  $SU(2)_L$  triplet  $\chi^a$  of Majorana fermions with zero hypercharge, as follows:

$$\mathcal{L}_{\text{triplet}} = \mathcal{L}_{\text{SM}} + i(\chi^a)^\dagger \bar{\sigma}_\mu \partial^\mu \chi^a - \frac{M}{2} \chi^a \chi^a + \mathcal{L}_5 + c_3 \left( H^\dagger \frac{\sigma^a}{2} H \chi^a \right)^2 + \text{h.c.} + \dots \quad (2.4)$$

As in the doublet case we assume a global symmetry which ensures the stability of the DM state,  $\chi^0$ . Here we have omitted the dimension-5 contributions to the triplet mass which only give rise to a global shift of the masses, while keeping the first non-trivial contribution to the mass splitting, which arises only at dimension 7. We would naively expect  $c_3$  to scale as  $g_*^4/M_*^3$ , resulting in a mass splitting:

$$\delta m = M_{\chi^\pm} - M_{\chi^0} = 2c_3 \frac{m_W^4}{g_L^4} \quad (2.5)$$

Taking weak coupling and new physics at the scale  $M_* \sim 4$  TeV as before, the tree-level contribution to the splitting is tiny,  $\delta m \sim 7$  MeV, in comparison with the contribution coming from electroweak loops. In the limit  $M \gg m_Z$  the latter yields  $\delta m = \alpha_L m_W \sin^2 \frac{\theta_W}{2} = 165$  MeV [21]. A large change in the splitting away from the electroweak loop value would therefore require strong coupling at a relatively low scale.

For the purposes of this work we will treat  $\delta m$  as a free parameter, allowing it to vary freely in the range  $[0, 1]$  GeV. For reasons that will become clear later we will be most interested in the regime where the total splitting is smaller than the one-loop correction. This requires a precise cancellation between the tree-level new physics contribution to the splitting and the one-loop electroweak correction, which in principle are parametrically unrelated, constituting a tuning. We will always require  $\delta m$  be positive, in order to have a good dark matter candidate. Note that in an abuse of nomenclature we will refer to the above two simplified models as the ‘pure Higgsino’ and ‘pure Wino’ scenarios; we thank the reader to keep in mind that we are allowing for an arbitrary charged-neutral splitting  $\delta m$ .

For completeness we collect the relevant annihilation matrices and non-relativistic potentials for the weak doublet and triplet simplified models in Appendix A. Many of these were taken from [7, 21, 22].

## 2.1 Electroweak Sommerfeld factors

We will be particularly interested in the Sommerfeld enhancement in the spin-0, charge-zero channel, which is the only relevant channel for computing the dark matter indirect-detection cross section. The nonrelativistic potential in this channel contains a mixing term between the charged-charged ( $\chi^+ \chi^-$ ) and neutral-neutral ( $\chi^0 \chi^0$ ) states:

$$V_{\text{doublet}} = \begin{pmatrix} 2\delta m - \frac{\alpha}{r} - \frac{\alpha_L}{r} \frac{(2c_W^2 - 1)^2}{4c_W^2} e^{-M_Z r} & -\frac{\alpha_L}{2r} e^{-M_W r} \\ -\frac{\alpha_L}{2r} e^{-M_W r} & -\frac{\alpha_L}{4c_W^2 r} e^{-M_Z r} \end{pmatrix} \quad (2.6)$$

$$V_{\text{triplet}} = \begin{pmatrix} 2\delta m - \frac{\alpha}{r} - \frac{\alpha_L c_W^2}{r} e^{-M_Z r} & -\sqrt{2} \frac{\alpha_L}{r} e^{-M_W r} \\ -\sqrt{2} \frac{\alpha_L}{r} e^{-M_W r} & 0 \end{pmatrix}$$

At small velocities,  $\beta \ll M/m_{W,Z}$ , we would expect the Sommerfeld factor in the neutral channel to show pure Yukawa-type behaviour, growing like  $1/\beta^2$  at masses where there is a zero-energy resonance and saturating to a constant away from the resonance as in Equation (1.16), with the size of the enhancement set by the distance from the resonance.

We will begin by examining this effect in the context of the more familiar Wino case. In the left panel of Figure 2, we plot numerical results for the Wino Sommerfeld factors in the charged-charged and neutral-neutral channels ( $S_1$  and  $S_2$ , respectively, as defined in Eq. (1.10) and computed for the total annihilation matrix) as a function of the relative velocity of the incoming neutral states,  $\beta$ , for Wino mass varying around the resonant value and nominal splitting. Since the velocity is defined with respect to the neutral states, the charged-charged Sommerfeld factor is zero below the pair-production threshold for the charged state,  $\beta_{\text{th}}$ , as explained in 1 and Equation (1.17). We expect the enhancement in this channel to grow with decreasing  $\chi^+$  velocity due to the Coulomb potential; this growth will be cut off by the non-Coulomb components of the interaction.

Also visible in this figure is the enhancement at specific velocities just below to the charged particle threshold, due to production at threshold of Coulomb ‘bound states’ of a charged DM pair. Approximating the binding energy  $E_n$  of the  $n$ th bound state as being purely due to the Coulomb interaction to leading order, we expect to see corresponding peaks in the Sommerfeld factor in the neutral channel at velocities:

$$\beta_n^* = \sqrt{\frac{2\delta m}{M} - \frac{\alpha^2}{4n^2}} \quad (2.7)$$

The true location of the peaks will depend on the energy levels of the bound states in the full electroweak potential. For Winos and Higgsinos with nominal mass splitting, the Coulomb resonances are squeezed in a narrow range of velocity just below the charged particles threshold, where the Sommerfeld factors display a complicated pattern of peaks and dips. The peaks can be large but are rather narrow in velocity<sup>4</sup>. Thus we expect the physical annihilation cross-section in the neutral channel to be enhanced at velocities just below the charged-particle threshold. We will come back to this point in our discussion of the Higgsino Sommerfeld factors below.

We can get some intuition for the Yukawa resonances by diagonalizing the potential in the pure  $SU(2)_L$  limit ( $\delta m \rightarrow 0$  and  $g_Y \rightarrow 0$ ) to go to the isospin basis. This yields one attractive and one repulsive eigenvalue in each case:

$$V_{\text{doublet}}^{\text{diag}} = \frac{\alpha_L}{4r} e^{-M_W r} \begin{pmatrix} 1 & 0 \\ 0 & -3 \end{pmatrix} \quad V_{\text{triplet}}^{\text{diag}} = \frac{\alpha_L}{r} e^{-M_W r} \begin{pmatrix} 1 & 0 \\ 0 & -2 \end{pmatrix} \quad (2.8)$$

Assuming the Sommerfeld factor to be dominated by the effect of the attractive Yukawa component, we can use the Hülthen potential approximation to obtain the Sommerfeld factor in analytical form, as well as an estimate of the mass at which the first zero-energy bound state arises. These are computed as  $M^* = (3/4\alpha_L)^{-1} k M_W = 5.25 \text{ TeV}$  ( $M^* = (2\alpha_L)^{-1} k M_W = 1.97 \text{ TeV}$ ) for the doublet (triplet) states; the closeness of the latter resonance mass to that of the thermal relic Wino that is responsible for the large enhancement to the indirect detection signal for the Wino [23, 24]. Instead, for the Higgsino the resonance mass is too far away from the allowed range of relic masses to have any significant effect.

---

<sup>4</sup>Here the tiny width of the resonance is due to decays of the Coulomb resonance to  $\chi_0\chi_0$  only, and doesn’t include decays to SM final states

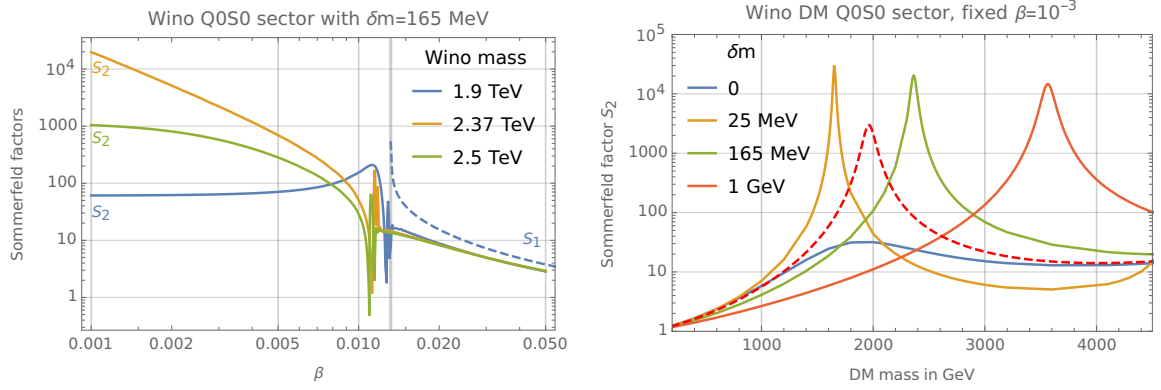


**Figure 2.** Sommerfeld factors for a pure Wino state. Left panel: Sommerfeld factors in the neutral (solid) and charged (dashed) channels as a function of DM velocity for various masses around to  $M^* \sim 2.37$  TeV, the position of the first zero-energy bound state. The charged-neutral splitting  $\delta m$  is fixed at the nominal electroweak-loop value, setting the position of the Coulomb resonances around  $\beta \sim 0.01$ . Right panel: Sommerfeld factor in the neutral channel computed at fixed velocity ( $\beta = 10^{-3}$ ) as a function of Wino mass for varying splitting charged-neutral  $\delta m$ . We see that the resonant mass  $M^*$  at which there is a zero-energy bound state varies with  $\delta m$ . We also show the analytical result for  $g_Y \rightarrow 0$  and zero splitting for comparison (dashed line).

In Figure 2, right panel we plot the analytical approximation to the Wino Sommerfeld enhancement at fixed, small velocity  $\beta = 10^{-3}$  as a function of Wino mass. For comparison we also show the numerical results for the full electroweak potential for various choices of charged-neutral splitting,  $\delta m$ . We see that varying the mass splitting shifts the zero-energy resonance to different values of the DM mass, away from the resonance position estimated using Equation (1.16). The dependence of the resonant mass on the splitting can be understood using perturbation theory [25].

The Sommerfeld factors for the pure Higgsino display similar features, but the details are rather different, see Figure 3. The left panel contains the variation of the Sommerfeld factor in the neutral-neutral channel with Higgsino mass, at  $\beta = 10^{-3}$  and for varying splitting, with the analytical result in the zero-hypercharge limit shown as a dashed red line. In the right panel we zoom in on the region around the charged-pair threshold for the thermal relic Higgsino (depicted as a solid black line) with small splitting  $\delta m = 9.5$  MeV, which allows us to clearly resolve the first three Coulomb resonances. The naive predictions for the velocities at which they are excited (using the pure Coulomb binding energies as in Equation (2.7)) are marked with vertical dashed lines, and are remarkably accurate. For the Wino this is not the case, the simple Coulomb approximation being off by approximately 20%. This is understandable in light of the larger weak Casimir factors that the Wino is subject to, being a triplet of  $SU(2)_L$ . A better approximation for the Coulomb resonances could be obtained by numerically solving the mixed Sommerfeld equation for the bound states.

## Relic density

It is well known that Sommerfeld enhancement has a significant effect on the Wino relic density, giving rise to a global increase in the annihilation cross section for the relic even away from the zero-energy resonance [8]. This is not true for the relic Higgsino [22]. Moreover, at freeze-out velocities  $x_F \sim 25$ , we are always in the regime where the mass splitting is

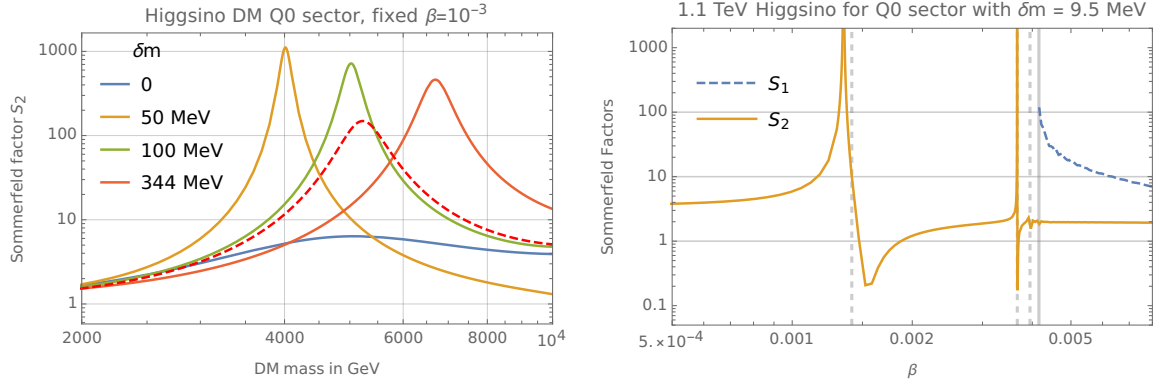


**Figure 3.** Sommerfeld factors for a pure Higgsino. Left panel: Sommerfeld factor in the neutral channel computed at fixed velocity ( $\beta = 10^{-3}$ ) as a function of Higgsino mass for varying charged-neutral splitting  $\delta m$ . The analytical result for  $g_Y \rightarrow 0$  and zero splitting is shown for comparison (dashed line). Right panel: zoom around the threshold region for a 1.1 TeV thermal relic Higgsino with splitting  $\delta m = 9.5$  MeV. The solid grey line indicates the charged particle pair-production threshold  $\beta_{th}$  and the grey dashed lines show the predicted positions of the first three Coulomb resonances.

negligible in comparison to the thermal kinetic energy  $\delta m \ll M\beta^2/2$ , ensuring that the splitting, and the related Coulomb resonances, have no effect on the thermal relic mass. The thermal Higgsino and Wino relic masses can thus be taken to be fixed at  $1070 \pm 10$  GeV and  $M = 2925 \pm 15$  GeV, respectively. We review details of the relic density calculation including Sommerfeld enhancement in appendix B.

### 3 Indirect detection

Constraints from the detection of SM products of annihilating or decaying dark matter today, or indirect detection, come from searches for gamma rays or antiprotons originating in dark-matter-rich regions within and without our galaxy. In this work we focus exclusively on gamma ray bounds, which have simpler propagation physics than the antiproton bounds and yield comparable limits for large dark matter masses [26] and cuspy profiles [27]. In particular we will constrain our simplified models using measurements of the continuum photon spectrum in the galactic centre due to HESS [28], and in dwarf spheroidal galaxies as given by the Fermi-LAT collaboration [29].

A continuum spectrum of photons comes mainly from the self-annihilation of DM ( $\text{DM DM} \rightarrow WW + ZZ$ ) and subsequent decay and radiation of the daughter electroweak gauge bosons. The flux of gamma rays from DM annihilation, as seen on the earth, depend on the so-called J-factor, the integral of the DM density over the line of sight to the source. The J-factor depends on the DM profile and its uncertainties. From the gamma ray measurement, knowing the spectrum of photons from the decay of  $WW, ZZ$  final states and taking into account J-factor uncertainties, one can extract bounds on the present-day thermally-averaged annihilation cross-section  $\langle \sigma \beta \rangle$  as function of the DM mass  $M$ . The galactic centre is the region with the higher expected DM density and thus has a large J-factor, however it is also home to important astrophysical gamma ray sources. The typical relative velocity of DM in our galaxy is predicted to be around  $\beta = 10^{-3}$ . In contrast, dwarf spheroidal satellite galaxies present less astrophysical background but have a lower J-factor. Furthermore the velocity

of DM particles in the dwarves halo is smaller than in our galaxy, around  $\beta = 10^{-5} - 10^{-4}$ . Since the present day DM velocity is very low, taking into account Sommerfeld enhancement for the computation of  $\langle\sigma\beta\rangle$  is crucial [24].

Today, all of the DM in the universe is neutral so the relevant annihilation process is  $\text{DM}^0 \text{DM}^0 \rightarrow WW + ZZ$ . In the absence of low-velocity resonances in the Sommerfeld factor, the enhancement saturates at a constant value and can be factorized out of the thermal average. The Sommerfeld-enhanced annihilation cross section can then be computed by simply multiplying the tree-level cross section by the value of the Sommerfeld factor at saturation. Provided saturation occurs above  $\beta \sim 10^{-3}$ , we will obtain equal annihilation cross section for both the galactic centre and dwarf galaxies [3].

In the presence of Coulomb resonances however, this is no longer the case, and we need to account for the spread in velocity of DM particles in calculating the thermally-averaged cross section. We do this by approximating the DM velocity as a thermal distribution, centred at  $\beta = 10^{-3}$  ( $x = 10^6$ ) for galactic signals, and  $\beta = 5 \times 10^{-5}$  ( $x = 4 \times 10^8$ ) for dwarf spheroidals.

We estimate that the annihilation cross section will receive a large enhancement in one of two scenarios: first when the dark matter mass is close to the resonant mass where there is a zero-energy bound state due to the Yukawa potential (this is the case for the thermal Wino with nominal splitting); and second, for any dark matter mass, when a Coulomb resonance coincides with the central value for the corresponding dark matter velocity distribution. As argued above, in our electroweakino examples this can only occur when the splitting is tuned to be of order the Coulomb binding energy. We can use the naive estimate in equation (2.7) to conclude that the indirect-detection signal due to pure Higgsinos in the galactic centre will receive a large boost at splittings  $\delta m \sim 9.0, 2.7$  MeV, due to Coulomb resonances with  $n = 1, 2$ . Similarly, solving for  $\beta \sim 5 \times 10^{-5}$  we can estimate a similar enhancement to the indirect-detection signal in dwarf galaxies at  $\delta m \sim 8.4, 2.1$  MeV. For larger splittings, the annihilation cross-section to  $WW$  and  $ZZ$  will remain an order of magnitude below the indirect detection bounds of HESS and Fermi-LAT [3].

This back-of-the-envelope estimate is borne out by the numerical results, presented in figure 4 for pure Higgsino mass close to the thermal relic value. For dark matter in the galactic centre (left panel), the annihilation cross-section stays roughly constant as we decrease the splitting until we reach  $\delta m \sim 20$  MeV. As we decrease the splitting still further we encounter a very narrow peak near  $\delta m = 9$  MeV that boosts the thermally-averaged cross section by two orders of magnitude. As we decrease the splitting even further, the  $n = 1$  Coulomb resonance crosses the  $\chi^0 \chi^0$  threshold and we lose the enhancement. The same phenomenon recurs around  $\delta m = 2$  MeV, where we encounter the  $n = 2$  resonance. For dwarf galaxies (right panel) the picture is even clearer. The figure shows two large but very narrow peaks slightly shifted in comparison to the ones for galactic centre measurements, but compatible with the values predicted by the naive formula.<sup>5</sup> From this we can conclude that for a pure Higgsino thermal relic, charged-neutral mass splittings in the range  $\delta m \in [8.5, 10.5]$  MeV and  $[2, 2.5]$  MeV are excluded by measurements of the indirect-detection cross-section by HESS. Similarly Fermi-LAT observations exclude a very narrow region around  $\delta m = 8.5$  MeV and around  $\delta m = 2.1$  MeV. These results are relatively stable under small variations in the

<sup>5</sup>Although these enhancements are large, they are well within the limit due to perturbative unitarity [30], being naturally cut off by the total width of the resonance. Note that in computing the Sommerfeld enhancement we only include the partial width to dark matter final states; we are therefore neglecting the further broadening of the resonance due to direct decays to SM final states.



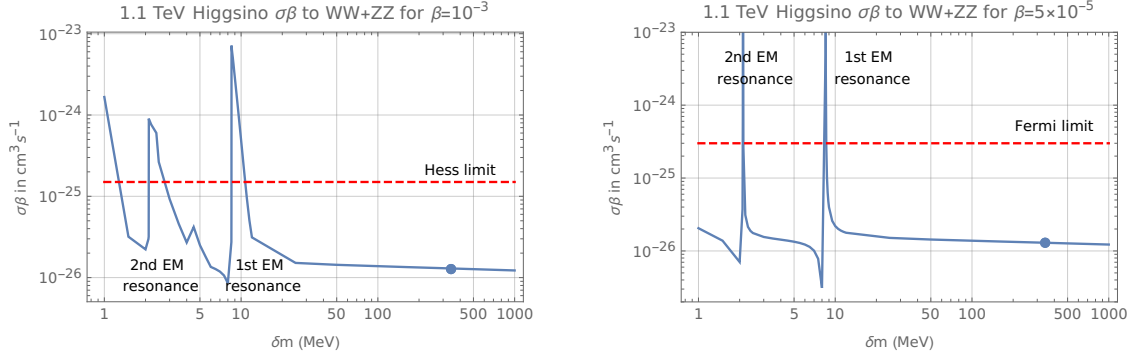


**Figure 4.** Thermally-averaged annihilation cross-section to  $WW + ZZ$  for a thermal relic Higgsino as a function of the charged-neutral splitting for: (left panel) galactic velocities  $\beta = 10^{-3}$  and (right) dwarf-spheroidal velocities  $\beta = 5 \times 10^{-5}$ . The red dashed lines are the experimental limits due to HESS (left) and Fermi-LAT (right), respectively, as taken from [3]. The nominal value for the splitting is shown as a large dot.

Higgsino mass.

The story for the thermal Wino is rather different. The annihilation cross section for a pure Wino thermal relic with nominal splitting receives a significant boost from Sommerfeld enhancement, due to its proximity to a zero-mass resonance, bringing it well above the bound from HESS, and comparable to that from Fermi-LAT. Note however that the HESS bound is computed using the Einasto profile for the halo density, which is cuspy towards the galactic centre, and using a cored profile would significantly relax this constraint [31].

Decreasing the charged-neutral splitting from the nominal value should shift the resonant mass (at which we see a zero-energy bound state) to lower values, further away from the thermal relic mass, thus decreasing the annihilation cross section. As the mass splitting gets smaller still, below  $\delta m \sim 20$  MeV, as estimated from equation (2.7), the first Coulomb resonance will come into play, again resulting in an enhanced cross section.

Numerical results for the thermally averaged annihilation cross-section for pure Wino mass around the thermal relic value are shown in figure 5. As before, dark matter today is taken to have a thermal velocity distribution centred on  $\beta = 10^{-3}$  for galactic centre measurements (left panel) and  $\beta = 5 \times 10^{-5}$  for Fermi-LAT measurements (right panel). As argued above, we see a range of intermediate splittings  $\delta m \in [20, 55]$  MeV for HESS measurements and  $\delta m \in [15, 200]$  MeV for Fermi-LAT, for which the annihilation cross section is smallest. Above this value, there is a large enhancement due to a zero-energy bound state held together by the Yukawa potential; below this value the enhancement is due to a Coulomb resonance. In this window the cross-section is around a factor of two below the HESS limit, well into the uncertainty band of the J-factor [28]. Varying the relic mass results in a small shift of this window.

Here we tuned the splittings to these specific, small values in order to probe regions where the effect due to Coulomb resonances is significant. One could instead envision a future where indirect-detection signals are measured in galaxies and clusters at many different scales, allowing us to ‘scan’ over a range of dark matter velocities in search of resonant effects.

We can study this possibility by computing the annihilation cross-section while varying the effective  $x$  of the thermal velocity distribution used in the thermal averaging procedure,

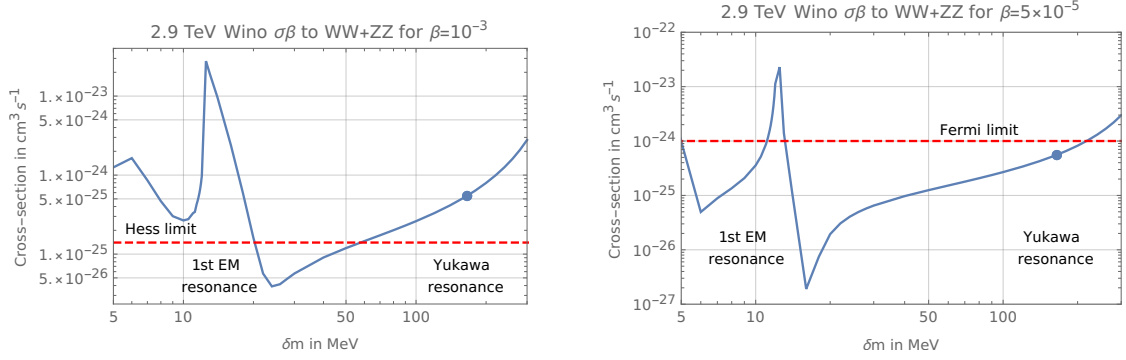


**Figure 5.** Thermally-averaged annihilation cross-section to  $WW + ZZ$  for a thermal relic Wino as a function of the charged-neutral mass splitting for: (left panel) galactic velocities  $\beta = 10^{-3}$  and (right) dwarf-spheroidal velocities  $\beta = 5 \times 10^{-5}$ . The red dashed lines are the experimental limits due to HESS (left) and Fermi-LAT (right), respectively, as taken from [3]. The nominal value for the splitting is shown as a large dot.

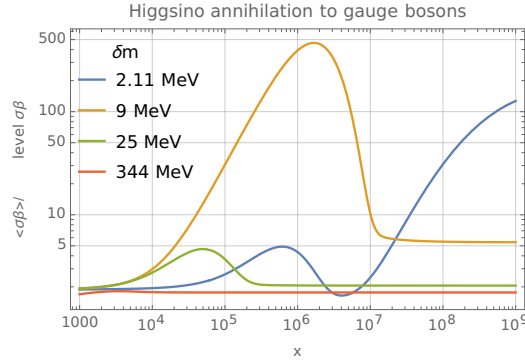


**Figure 6.** Thermally-averaged annihilation cross section for 1.1 TeV pure Higgsino for some discrete values of the charged-neutral mass splitting  $\delta m$ . The thermal average is computed using a Maxwell-Boltzman distribution for the dark matter velocity, centred at varying  $x$ , in order to mimic potential future measurements taken in galaxies and clusters of different scales.

to mimic results due to dark matter in clusters of different scales. In figure 6 we show the variation of the sommerfeld-enhanced, thermally-averaged annihilation cross section for a 1.1-TeV pure Higgsino with  $x$  in the dark matter distribution (see equation (B.5)). The same large enhancements at  $\delta m = 2.1, 9$  MeV are also visible here, at  $x$  corresponding to the average dark matter velocity in dwarf galaxies, and the galactic centre, respectively. As the splitting grows, we see the resonance moving to lower values in  $x$ , corresponding to larger cluster sizes. Measuring the continuum signal in galactic clusters with  $x \sim 4 \times 10^4$ , for example, would allow us to probe Higgsino mass splittings  $\delta m \sim 25$  MeV. However increasing the splitting moves the resonances to larger velocities, resulting in smaller enhancements which can be washed out in the thermal average. The enhancement for 25-MeV splitting is just a factor of 5 at its maximum, whereas for nominal splitting there are many resonances that are rather close together, and the enhancement is washed out entirely in the thermal average.



In principle we should include thermal effects in the above computations, the main consequence of which would be to cut off the Coulomb enhancement in the charged channel due to the thermal mass of the photon. We have verified that this has a negligible effect on the results quoted above. Resummation of additional thermal effects that could lead to e.g. mixing between scattering states and bound states in the presence of a thermal plasma, have also been computed [32, 33], although it is currently unclear whether these plays a significant role in electroweakino annihilation.

## 4 Two complete models

In this section we embed the pure weakinos with variable mass splitting in two more complete models of new physics: the MSSM, and  $N = 2$  SUSY with Dirac gauginos, in order to determine the consistent range of variation of the charged-neutral splitting  $\delta m$  in these models.

### 4.1 MSSM

The MSSM is the canonical example of a more complete model in which the pure doublet and triplet weakinos can be realized in different corners of its parameter space. In addition if the weakino is the lightest supersymmetric particle (LSP), it is automatically stable in the  $R$ -parity-conserving limit. In the fermionic sector of the MSSM, the neutral Higgsinos  $\tilde{H}_u^0$  and  $\tilde{H}_d^0$  mix with the neutral electroweak gauginos  $\tilde{B}, \tilde{W}^0$  to form four neutralinos, and the charged components of the Higgsinos and Wino also mix, yielding two charginos. In the gauge eigenstate basis  $\psi_{\tilde{N}} = (\tilde{B}, \tilde{W}^0, \tilde{H}_u^0, \tilde{H}_d^0)$ , the neutralino mass matrix is [34]:

$$M_{\tilde{N}} = \begin{pmatrix} M_1 & 0 & -c_\beta s_W m_Z & s_\beta s_W m_Z \\ 0 & M_2 & c_\beta c_W m_Z & -s_\beta c_W m_Z \\ -c_\beta s_W m_Z & c_\beta c_W m_Z & 0 & -\mu \\ s_\beta s_W m_Z & -s_\beta c_W m_Z & -\mu & 0 \end{pmatrix} \quad (4.1)$$

In order to avoid large CP-violating effects in the Higgs sector, we restrict ourselves to real mass parameters  $\mu, M_1, M_2$  but we allow for one non-trivial relative sign between them.

The chargino mass matrix in the gauge-eigenstate basis  $\psi_{\tilde{C}} = (\tilde{W}^+, \tilde{H}_u^+, \tilde{W}^-, \tilde{H}_d^-)$  is, in block form:

$$M_{\tilde{C}} = \begin{pmatrix} 0 & X^T \\ X & 0 \end{pmatrix} \quad \text{where} \quad X = \begin{pmatrix} M_2 & \sqrt{2}s_\beta m_W \\ \sqrt{2}c_\beta m_W & \mu \end{pmatrix} \quad (4.2)$$

### Higgsino limit

In the pure Higgsino limit,  $M_1, M_2 \rightarrow \infty$ , the Wino and Bino decouple giving two neutralinos and one chargino state, all with the same tree-level mass:

$$m_{\tilde{N}_1} = m_{\tilde{N}_2} = m_{\tilde{C}_1} = \mu \quad (4.3)$$

The two neutralino can be combined into a single Dirac fermion Higgsino, of mass  $\mu$ .

Instead in the limit of large finite  $M_1, M_2$  we can integrate out the heavy Wino and Bino at tree-level to obtain

$$\mathcal{L}_{\text{eff}} = \frac{g_Y^2}{4M_1} (h_u^* \tilde{H}_u - h_d^* \tilde{H}_d)^2 + \frac{g_L^2}{4M_2} (h_u^* \sigma^a \tilde{H}_u + h_d^* \sigma^a \tilde{H}_d)^2 + c.c. \quad (4.4)$$

Note that this contains lepton-number-violating terms which were not considered in the simplified model for the doublet, equation (2.1). Setting the scalar Higgses to their VEVs, we get the following masses at first order in  $m_W/M_1$ ,  $m_W/M_2$ :

$$m_{\tilde{N}_{1,2}} = |\mu| - \frac{\sin 2\beta}{2} \frac{\mu}{|\mu|} \left( \frac{m_Z^2 s_W^2}{M_1} + \frac{m_W^2}{M_2} \right) \pm \frac{1}{2} \left| \frac{m_Z^2 s_W^2}{M_1} + \frac{m_W^2}{M_2} \right| + O\left(\frac{m_W^2}{|M_1|^2}, \frac{m_W^2}{|M_2|^2}\right) \quad (4.5)$$

$$m_{\tilde{C}_1} = |\mu| - \sin 2\beta \frac{\mu}{|\mu|} \frac{m_W^2}{M_2} + O\left(\frac{m_W}{|M_2|^2}\right) \quad (4.6)$$

The tree-level mass splitting between the lightest chargino and lightest neutralino is given by

$$\delta m_{\text{tree}} = m_{\tilde{C}_1} - m_{\tilde{N}_1} = \frac{\sin 2\beta}{2} \frac{\mu}{|\mu|} \left( \frac{m_Z^2 s_W^2}{M_1} - \frac{m_W^2}{M_2} \right) + \frac{1}{2} \left| \frac{m_Z^2 s_W^2}{M_1} + \frac{m_W^2}{M_2} \right| + O\left(\frac{m_W^2}{|M_1|^2}, \frac{m_W^2}{|M_2|^2}\right) \quad (4.7)$$

There is also a splitting between the two neutral Majorana states, generated at the same order:

$$\delta m_0 = M_{\tilde{N}_2} - M_{\tilde{N}_1} = m_Z^2 \left| \frac{s_W^2}{M_1} + \frac{c_W^2}{M_2} \right| + O\left(\frac{m_W^2}{|M_1|^2}, \frac{m_W^2}{|M_2|^2}\right) \quad (4.8)$$

A neutral splitting  $\delta m_0 > \mathcal{O}(100)$  KeV, allows the pure the pure Higgsino to evade the strong bound from direct detection due to  $Z$ -exchange. We neglected the effect of a non-zero  $\delta m_0$  in our numerical calculations even though it is parametrically of the same order as the charged-neutral mass splitting  $\delta m$ . We expect that taking it into account will not change our main conclusion, although it will shift the precise position of the Coulomb resonances. The effect of the neutral-neutral mass splitting on Sommerfeld enhancement is investigated in [35].

We see from equation (4.7) that when  $M_1$  and  $M_2$  have opposite sign, their contributions to the splitting partially cancel. For  $\mu > 0$  one can have a negative tree-level contribution to the splitting for  $M_1$  negative and  $M_2$  positive provided that:

$$-M_2 \tan^2 \theta_W \frac{1 + \sin 2\beta}{1 - \sin 2\beta} < M_1 < -M_2 \tan^2 \theta_W \frac{1 - \sin 2\beta}{1 + \sin 2\beta} \quad (4.9)$$

This region is the entire quadrant  $M_1 < 0$ ,  $M_2 > 0$  when  $\tan \beta = 1$  and narrows to the line of equation  $M_1 = -M_2 \tan^2 \theta_W$  as  $\tan \beta$  goes to infinity.

We plot the total charged-neutral mass splitting, including the electroweak loop contribution, in figure 7 for different values of  $\tan \beta$ . As in the simplified, for fixed  $M_2$  the maximum possible range for the splitting is the interval  $\delta m = \pm \frac{m_W^2}{M_2}$ , and we see that it can be much smaller than the electroweak loop value within the MSSM parameter space, justifying our taking  $\delta m$  varying in the range  $[0, 1.5 \text{ GeV}]$ .

## Wino limit

In the pure Wino limit  $\mu, M_1 \rightarrow \infty$  the Bino and Higgsino decouple from the theory and we are left with a Majorana neutralino and a Dirac chargino that are degenerate in mass:

$$m_{\tilde{N}_1} = m_{\tilde{C}_1} = M_2 \quad (4.10)$$

For finite  $\mu$ ,  $M_1$  we can again integrate out the Higgsino and Bino at tree-level to obtain

$$\mathcal{L}_{\text{eff}} = -\frac{g_L^2}{2\mu} h_u^* \cdot h_d^* \widetilde{W}^a \widetilde{W}^a + \frac{g_L^2 g_Y^2}{2M_1 \mu^2} \left( h_u^* \cdot (h_d^* \sigma^a) \widetilde{W}^a \right)^2 \quad (4.11)$$

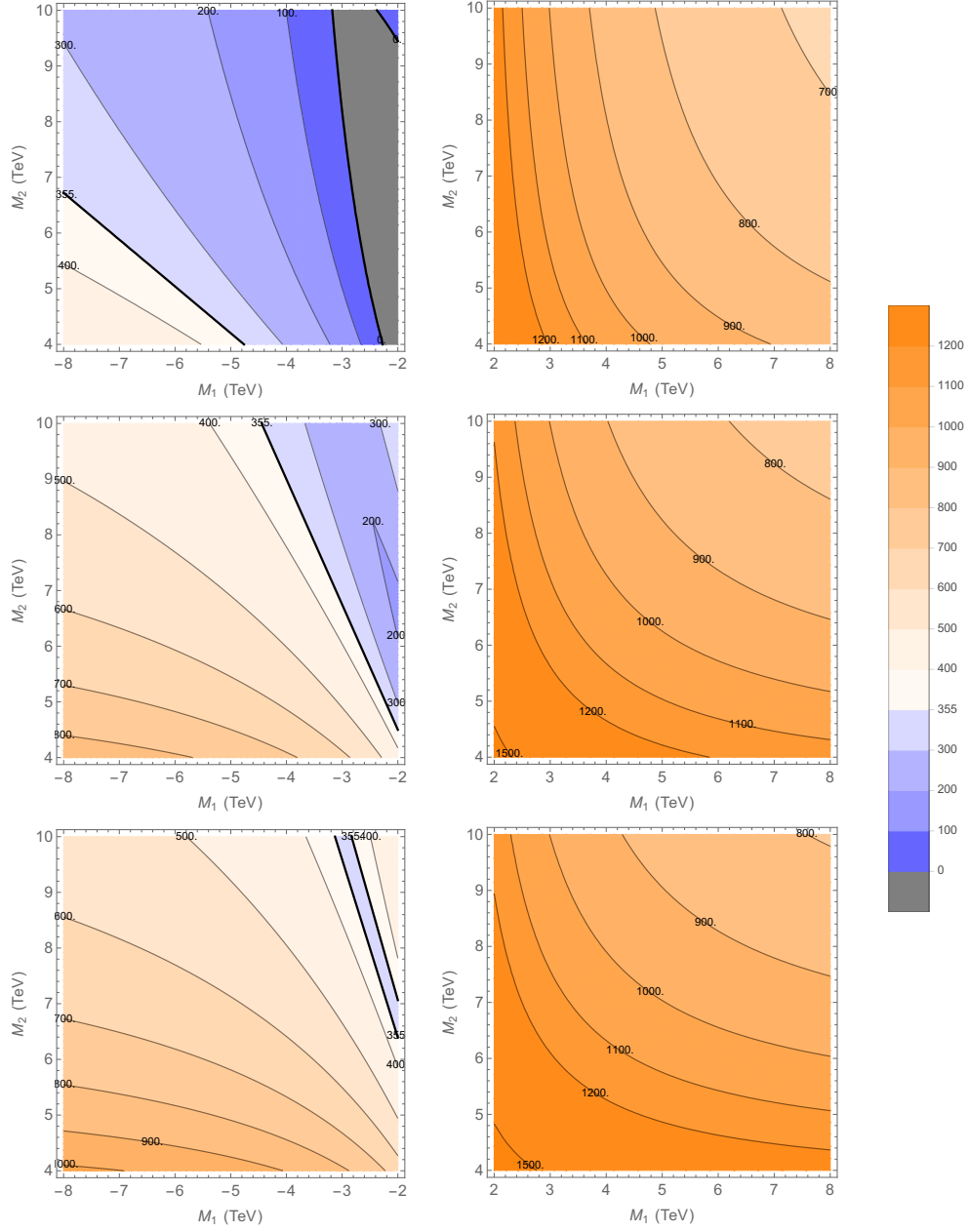


**Figure 7.** Contours of the total charged-neutral mass splitting  $\delta m$ , in MeV, in the pure Higgsino limit of the MSSM as a function of  $M_1$  and  $M_2$ , for  $\tan \beta = 3$  (top),  $\tan \beta = 10$  (middle) and  $\tan \beta = 80$  (bottom).

Setting the Higgses to their VEVs, we get the following masses:

$$\begin{aligned}
 m_{\tilde{N}_1} &= M_2 - \frac{m_W^2}{\mu} \sin 2\beta - \frac{m_W^4}{\mu^2 M_1} \sin^2 2\beta \tan^2 \theta_W + \dots \\
 m_{\tilde{C}_1} &= M_2 - \frac{m_W^2}{\mu} \sin 2\beta + \dots
 \end{aligned}
 \tag{4.12}$$

As in the simplified model, the mass splitting is only affected by the dimension seven operator. Explicitly:

$$\delta m_{\text{tree}} = m_{\tilde{C}_1} - m_{\tilde{N}_1} = \frac{m_W^4}{\mu^2 M_1} \sin^2 2\beta \tan^2 \theta_W \quad (4.13)$$

which can be negative, for  $M_1 < 0$ . However for any reasonable hierarchy of masses, this tree-level contribution is negligible compared with the electroweak loop contribution. The MSSM in the Wino limit behaves essentially like a pure weak-triplet fermion with charged-neutral splitting fixed at 165 MeV. As explained in Section 2 generating a splitting parametrically smaller than the nominal value will require strong coupling at a few TeV.

## 4.2 Dirac gaugino

It is possible to obtain something closer to the weak doublet simplified model used in this work, with a neutral splitting  $\delta m_0$  that is parametrically smaller than the charged-neutral splitting  $\delta m$ , in a scenario with Dirac gauginos, coming from  $N = 2$  SUSY, as described in detail in [36]. We summarize the relevant results of this paper below.

Adding to the MSSM chiral superfields transforming in the adjoint representation of the gauge group: a triplet  $T$  for  $SU(2)_L$  and a singlet  $S$  for  $U(1)_Y$ , allows us to write down Dirac mass terms for the gauginos:

$$\mathcal{L} = -m_{1D} \tilde{S} \tilde{B} - m_{2D} \tilde{T}^a \tilde{W}^a + c.c. \quad (4.14)$$

Futhermore, we add to the MSSM superpotential all interactions that are compatible with the symmetries

$$W = \frac{M_S}{2} S^2 + \lambda_S S H_d \cdot H_u + \frac{M_T}{2} T^a T^a + \lambda_T T^a H_d \cdot \frac{\sigma^a}{2} H_u \quad (4.15)$$

as well as soft masses for the adjoint superfields, forming a neutralino sector with six Majorana fermions  $\tilde{B}, \tilde{S}, \tilde{W}^3, \tilde{T}^3, \tilde{H}_u^0, \tilde{H}_d^0$ .

If we take these superfields to arise from a  $N = 2$  supersymmetric multiplet, then the superpotential couplings take the value  $\lambda_S = \sqrt{2} g_Y / 2$  and  $\lambda_T = \sqrt{2} g_L / 2$ . Keeping only the Dirac mass terms, the neutralinos form three Dirac fermions. If we now take the Higgsino limit  $m_{1D}, m_{2D} \rightarrow \infty$ , we are left with an Dirac electroweak doublet chargino-neutralino of mass  $|\mu|$  and with mass splitting given at first order by:

$$\delta m = \cos 2\beta m_Z^2 \left( \frac{s_W^2}{m_{1D}} - \frac{c_W^2}{m_{2D}} \right) \quad (4.16)$$

However, if we consider that  $\lambda_S$  and  $\lambda_T$  take their value at some  $N = 2$  scale  $M_{N=2}$  then the running of the couplings down to the supersymmetry breaking scale are different for  $\lambda_S, \lambda_T$  than for  $g_L, g_Y$  because the adjoint fields do not couple to SM matter. This generates a neutral-neutral splitting given by the following equation in the Higgsino limit [36]:

$$\delta m_0 = 2s_\beta c_\beta \mu m_Z^2 \left[ \frac{c_W^2}{m_{2D}^2} \left( 1 - \frac{2\lambda_T^2}{g_L^2} \right) + \frac{s_W^2}{m_{1D}^2} \left( 1 - \frac{2\lambda_S^2}{g_Y^2} \right) \right] \quad (4.17)$$

Neglecting all SM couplings except the top Yukawa, this is given by:

$$\delta m_0 = 2s_\beta c_\beta \mu m_Z^2 \frac{3y_t^2}{8\pi^2} \log \left( \frac{M_{N=2}}{M_{N=1}} \right) \left[ \frac{c_W^2}{m_{2D}^2} + \frac{s_W^2}{m_{1D}^2} \right] \quad (4.18)$$

so that  $\delta m_0$  is suppressed compared to  $\delta m$  by a factor:

$$\frac{3y_t^2}{8\pi^2} \log\left(\frac{M_{N=2}}{M_{N=1}}\right) \left(\frac{\mu}{m_{1D,2D}}\right) \sim 10^{-2} \log\left(\frac{M_{N=2}}{M_{N=1}}\right) \quad (4.19)$$

for  $\mu = 1$  TeV and  $m_{1D,2D} \sim 4$  TeV. Then if we want the UV contribution to the charged neutral splitting to be of the order of the one-loop SM contribution in order to have  $\delta m$  in the 10 MeV region like in Section 4.1, the neutral-neutral splitting remains of the order of a few MeV.

## 5 Conclusion

In this paper we explored the effect on Sommerfeld enhancement of varying the splitting between the charged and neutral components of an electroweak-multiplet dark matter candidate, focusing on pure Higgsino and Wino dark matter for concreteness, and adding to the simplified model higher-dimension operators with variable Wilson coefficient that govern the splitting. We find as expected that the thermal relic density is unaffected by the charged-neutral splitting provided this is much smaller than the freeze-out temperature.

For indirect detection of dark matter the story is much more interesting, as the Sommerfeld enhancement is strongly sensitive to the presence of resonances, whose effect in a multi-state system changes with the splitting. We found that this statement doesn't only apply to the familiar 'zero-energy' Yukawa resonances responsible for enhancement of the Wino indirect detection signal, but also Coulomb resonances, or quasi-bound states of  $\chi^+\chi^-$ , the charged components of the dark matter multiplet. There is an infinite tower of such resonances lying between the free neutral two-particle state (ground state) and the charged particle threshold. When the incoming dark matter particles have just enough energy to create these states, their annihilation cross section is resonantly enhanced as in the usual Wino case. However unlike that due to a 'zero-energy' resonance, this enhancement only occurs for certain specific values of the incoming velocity that match the mass difference between the ground state and any of these Coulomb resonances.

For a pure Wino/Higgsino state with nominal splitting, the Coulomb binding energies  $E_{B,\gamma} = \alpha^2 M_\chi / (4n^2)$  for the charged state are negligible compared with the EW loop-induced charged-neutral splittings  $\delta m \sim \alpha m_Z$ , making the tower of Coulomb resonances hard to resolve, and the corresponding resonant velocities ( $\beta \approx 0.01/\beta \approx 0.025$ ) irrelevant for any measurable physical processes. Nevertheless in any scenario where the Coulomb binding energy is of the order of the splitting, these resonances can be easily resolved, and the lowest-lying resonances be brought close enough to the ground state to give a large boost to the indirect detection signal for dark matter today. For pure Higgsino dark matter we found that for multiple ranges of (small) splittings, of order the Coulomb binding energies of the  $\chi^+\chi^-$  bound state, the large boost to the indirect detection cross section at specific velocities relevant to those of dark matter today results in strong exclusions from continuum photon measurements, by HESS measurements in our galactic centre, and/or by Fermi-LAT measurements in dwarf spheroidal galaxies. We would expect a similar enhancement to the gamma-ray line signal. Conversely, we found that decreasing the splitting in the pure Wino scenario detunes the Yukawa resonance away from the ground state, relaxing the indirect detection constraints on the thermal Wino.

Although interesting, these results are of limited value in themselves: decreasing the charged-neutral splitting without making the charged state the lightest in the spectrum

requires an unnatural tuning between the contribution of a tree-level higher-dimension operator and that due to an electroweak loop. In the pure Wino case there is the additional complication that the leading tree-level operator affecting the splitting has mass dimension seven; making this contribution of the same order as the loop correction will require some strongly-coupled new physics. Furthermore electroweak multiplets with such small charged-neutral splittings will already be strongly constrained, perhaps even excluded, both by collider searches such as [37], as well as by capture and decay/annihilation of the heavy state in dense objects like the sun [38].

Instead we highlight the mechanism brought to light in this work which is rather generic, and will apply in any scenario where the dark matter two-to-two scattering contains an inelastic channel to a final state with constituents that are acted upon by a long-range force. In analogy with the electroweakino example detailed above, this will give rise to resonances that lie below the energy threshold for final-state production due to the formation of ‘Coulombic’ quasi-bound states, which are excited at specific incoming velocities of the annihilating dark matter, thus enhancing the annihilation cross section. However in the pure electroweakino case both the nominal charged-neutral splitting and the Coulomb binding energies are set by the same interaction and are rather disparate in size, requiring a tuning to make the resonance velocities relevant to existing measurements. This does not have to be the case more generally; the two relevant quantities could be unrelated, or could be naturally of the same order, which would automatically excite the Coulomb resonances at relevant velocities.

One could also invert this logic: rather than dialling the splitting between dark matter and its long-range interacting neighbour to ‘tune in’ the dark matter annihilation signal in the particular regions of the universe where we have already made measurements, we could more ambitiously envision the universe as a dark matter spectroscope, with the different scales at which dark matter clusters today playing the part of the dial. Measuring the indirect-detection signals in clusters at different scales would allow us to ‘tune’ this dial in search of a signal. If the dark matter sector contains some complex structure this should result in the spectroscope lighting up at specific ‘frequencies’, giving us detailed information on the dark matter energy spectrum.

This work opens up various directions of study which could be fruitful to pursue. Further to [25] it would be interesting to have an analytical estimate of the size and widths of, and interplay between, the different types of resonance; both the short-range Yukawa bound states and the long-range Coulomb ones. This would require solving the full mixed  $S = 0, Q = 0$  channel analytically (perhaps perturbatively) and would yield corrections to our naive estimates for the Coulomb/Yukawa resonance binding energies due to the other force. We hope this would also tell us why the analytic estimate in the  $g', \delta m \rightarrow 0$  limit works so well in the full mixed case for the Wino (but only for nominal splitting), and not at all for the Higgsino. In addition we have not included the contribution to the annihilation of the true formation and decay of the Coulomb bound state here. Unlike the Yukawa bound states, these are not the lowest-energy states in the system, and can be produced without requiring extra radiation. Moreover real Coulombic bound states will have additional decay channels to Standard Model final states, that are not taken into account here. Finally it would be entertaining to find an alternative dark sector framework in which the correct resonant velocities emerge naturally. Answering these questions would allow us to slowly piece together the puzzle, bringing us one step closer to understanding the nature and composition of the dark horse that is dark matter.

## Acknowledgements

We would like to give special thanks to Riccardo Rattazzi for his insightful guidance and frequent helpful discussions. RM thanks Matthew McCullough, John Ellis, Andrzej Hryczuk, Sasha Monin, Paolo Panci, Michele Redi, Tracy Slatyer and Kathryn Zurek for useful discussions, and CERN and EPFL, as well as the Galileo Galilei Institute for Theoretical Physics for their gracious hospitality during the completion of this project. KM thanks Laurent Vanderheyden for his help. RM was partially supported by the Swiss National Science Foundation under MHV grant 171330, and also thanks the État de Genève for its generous financial support.

## A Annihilation matrices

### Weak doublet (pure Higgsino)

Neglecting the mass splitting and all SM particle masses with respect to the large dark matter mass  $M$ , we get the following tree-level annihilation cross-section in the center of mass frame, in the non-relativistic limit:

$$\sigma(\text{DM} \overline{\text{DM}} \rightarrow \text{SM}) = \frac{\pi}{256M^2\beta} \left[ (81\alpha_L^2 + 12\alpha_L\alpha_Y + 43\alpha_Y^2) - \left( 90\alpha_L^2 - 12\alpha_L\alpha_Y + \frac{158}{3}\alpha_Y^2 \right) \beta^2 + O(\beta^4) \right] \quad (\text{A.1})$$

where  $\beta$  is the dark matter velocity in the centre-of-mass frame of the annihilating states.

For the purposes of computing the Sommerfeld enhancement, we express the  $s$ -wave ( $l = 0$ ) contribution in terms of an ‘annihilation matrix’  $\Gamma$  (the absorptive part of the two-to-two cross section) in independent sectors with differing electric charge:

$$\Gamma_{Q=0} = \frac{\pi\alpha_L^2}{256M^2} \begin{pmatrix} 31 + 4t_W^2 + 43t_W^4 & -22 - 4t_W^2 + 43t_W^4 \\ -22 - 4t_W^2 + 43t_W^4 & 31 + 4t_W^2 + 43t_W^4 \end{pmatrix} \quad (\text{A.2})$$

$$\Gamma_{Q=1} = \frac{\pi\alpha_L^2}{128M^2} (25 + 4t_W^2) \quad (\text{A.3})$$

and also compute the nonrelativistic potential due to gauge boson exchange in the different sectors:

$$V_{Q=0} = \begin{pmatrix} 2\delta m - \alpha_{em}/r - \alpha_L(2c_W^2 - 1)^2 e^{-M_Z r}/4rc_W^2 & -\alpha_L e^{-M_W r}/2r \\ -\alpha_L e^{-M_W r}/2r & -\alpha_L e^{-M_Z r}/4rc_W^2 \end{pmatrix} \quad (\text{A.4})$$

$$V_{Q=1} = \frac{\alpha_L}{r} e^{-M_Z r} \frac{2c_W^2 - 1}{4c_W^2} \quad (\text{A.5})$$

where we have used the shorthand notation  $c_W = \cos \theta_W$  and  $t_W = \tan \theta_W$ . Then the total annihilation cross-section is given by<sup>6</sup>:

$$\sigma\beta = (\sigma_{Q=0})_1 + (\sigma_{Q=0})_2 + 2\sigma_{Q=1} \quad (\text{A.6})$$

where the  $\sigma_Q$  are obtained by Equation (1.9) and the factor 2 comes from the counting of initial states.

---

<sup>6</sup>The average over the different species of DM particles and their spin is already included in the  $\Gamma$  for the relic calculation.

Separating out the annihilation to weak gauge bosons for the purposes of computing the indirect-detection signal:

$$\begin{aligned}\Gamma_{WW} &= \frac{\pi\alpha_L^2}{8M^2} \begin{pmatrix} 1 & 1 \\ 1 & 1 \end{pmatrix} & \Gamma_{ZZ} &= \frac{\pi\alpha_L^2}{16M^2 \cos^4 \theta_W} \begin{pmatrix} (1-2\sin^2 \theta_W)^4 & (1-2\sin^2 \theta_W)^2 \\ (1-2\sin^2 \theta_W)^2 & 1 \end{pmatrix} \\ \Gamma_{\gamma\gamma} &= \frac{\pi\alpha_{\text{em}}^2}{M^2} \begin{pmatrix} 1 & 0 \\ 0 & 0 \end{pmatrix} & \Gamma_{\gamma Z} &= \frac{\pi\alpha_L \alpha_{\text{em}}}{2M^2 \cos^2 \theta_W} \begin{pmatrix} (1-2\sin^2 \theta_W)^2 & 0 \\ 0 & 0 \end{pmatrix}\end{aligned}\quad (\text{A.7})$$

### Weak triplet (pure Wino)

For the weak triplet, the total annihilation cross section in the nonrelativistic limit, again neglecting SM masses and inter-state mass splittings is:

$$\sigma(\text{DM DM} \rightarrow \text{SM}) = \frac{\pi\alpha_L^2}{24M^2\beta} [37 - 20\beta^2 + O(\beta^4)] \quad (\text{A.8})$$

For the purposes of the Sommerfeld computation, the  $s$ -wave contribution to DM-DM annihilation can be split up into five independent sectors with total charge  $Q = 0, 1, 2$  and total spin  $S = 0, 1$  [22]. The corresponding annihilation and potential matrices are given below.

- $S = 0$  ,  $Q = 0$ . (This is the only sector containing mixing between two different two-particle states  $\text{DM}^+\text{DM}^-$  and  $\text{DM}^0\text{DM}^0$ ):

$$\Gamma_{Q=0}^{S=0} = \frac{\pi\alpha_L^2}{36M^2} \begin{pmatrix} 3 & \sqrt{2} \\ \sqrt{2} & 2 \end{pmatrix} \quad V_{Q=0}^{S=0} = \begin{pmatrix} 2\delta m - A & -\sqrt{2}B \\ -\sqrt{2}B & 0 \end{pmatrix} \quad (\text{A.9})$$

- $S = 1$  ,  $Q = 0$  ( $\text{DM}^+\text{DM}^-$ ):

$$\Gamma_{Q=0}^{S=1} = \frac{25\pi\alpha_L^2}{144M^2} \quad V_{Q=0}^{S=1} = 2\delta m - A \quad (\text{A.10})$$

- $S = 0$  ,  $Q = 1$  ( $\text{DM}^+\text{DM}^0$  and charged conjugate):

$$\Gamma_{Q=1}^{S=0} = \frac{\pi\alpha_L^2}{36M^2} \quad V_{Q=1}^{S=0} = \delta m + B \quad (\text{A.11})$$

- $S = 1$  ,  $Q = 1$  ( $\text{DM}^+\text{DM}^0$  and charged conjugate):

$$\Gamma_{Q=1}^{S=1} = \frac{25\pi\alpha_L^2}{144M^2} \quad V_{Q=1}^{S=1} = \delta m - B \quad (\text{A.12})$$

- $S = 0$  ,  $Q = 2$  ( $\text{DM}^+\text{DM}^+$  and charged conjugate):

$$\Gamma_{Q=2}^{S=0} = \frac{\pi\alpha_L^2}{36M^2} \quad V_{Q=2}^{S=0} = 2\delta m + A \quad (\text{A.13})$$

where we have defined:

$$A = \frac{\alpha_{em}}{r} + \frac{\alpha_L c_W^2}{r} e^{-M_Z r} \quad \text{and} \quad B = \frac{\alpha_L}{r} e^{-M_W r} \quad (\text{A.14})$$



Then the total annihilation to SM particles is given by:

$$\sigma\beta = 2(\sigma_{Q=0}^{S=0})_1 + (\sigma_{Q=0}^{S=0})_2 + 2\sigma_{Q=0}^{S=1} + 4\sigma_{Q=1}^{S=0} + 4\sigma_{Q=1}^{S=1} + 2\sigma_{Q=2}^{S=0} \quad (\text{A.15})$$

where the  $\sigma_Q^S$  are given by Equation (1.9). The additional multiplicative factors come from the counting of initial states.

The annihilation matrices to gauge boson final states used for computing the indirect detection cross-section are also given in [7]:

$$\begin{aligned} \Gamma_{WW} &= \frac{\pi\alpha_L^2}{8M^2} \begin{pmatrix} 2 & \sqrt{2} \\ \sqrt{2} & 4 \end{pmatrix} & \Gamma_{ZZ} &= \frac{\pi\alpha_L^2}{2M^2} \begin{pmatrix} \cos^4\theta_W & 0 \\ 0 & 0 \end{pmatrix} \\ \Gamma_{\gamma\gamma} &= \frac{\pi\alpha_{em}^2}{2M^2} \begin{pmatrix} 1 & 0 \\ 0 & 0 \end{pmatrix} & \Gamma_{\gamma Z} &= \frac{\pi\alpha_L\alpha_{em}}{2M^2} \begin{pmatrix} 2\cos^2\theta_W & 0 \\ 0 & 0 \end{pmatrix} \end{aligned} \quad (\text{A.16})$$

These are normalized differently to the ones in (A.9)-(A.13) because only the neutral state is present today.

## B Relic density calculation

In the standard thermal DM scenario, the DM particles are in thermal equilibrium with the SM particles in the early universe. As the universe expands, their number density is given by the Boltzmann equation:

$$\frac{dn}{dt} + 3Hn = -\langle\sigma\beta\rangle_{12}(n^2 - n_{eq}^2) \quad (\text{B.1})$$

where  $H$  is the expansion rate of the universe and  $\langle\sigma\beta\rangle_{12}$  the thermal average of the annihilation cross-section of DM particles to SM states multiplied by their relative velocity. When the temperature of the universe decreases below the DM mass  $M$ , its equilibrium density drops exponentially and the annihilation rate  $\Gamma = n\langle\sigma\beta\rangle_{12}$  becomes negligible compared to  $H$ . The DM particles are too rare to annihilate and their density is only diluting with the expansion of the universe. The temperature at which the DM particles decouple from the thermal bath is called the freeze-out temperature  $T_F$ .

Following the procedure described in [39], the thermal relic abundance of DM is given by:

$$\Omega_{\text{DM}}h^2 = \sqrt{\frac{45}{\pi}} \frac{s_0}{\rho_c} \frac{1}{\sqrt{g_*}M_P} \left[ \int_{x_F}^{\infty} \frac{\langle\sigma\beta\rangle_{12}}{x^2} dx \right]^{-1} \quad (\text{B.2})$$

where  $s_0 = 2891 \text{ cm}^{-3}$  is the entropy density today,  $\rho_c = 1.054 \times 10^{-5} h^2 \text{ GeV cm}^3$  is the critical density of the universe (values taken from [40]),  $x_F = \frac{M}{T_F}$  and  $g_*$  is the number of degrees of freedom at freeze-out. Since we expect  $T_F$  to be around 50 GeV we will take  $g_* = 92$  in all the following calculations. The freeze-out temperature is computed recursively with the formula:

$$x_F = \log \left[ \frac{5}{4} \sqrt{\frac{45}{\pi}} \frac{g}{8} \frac{M M_P}{2\pi^3 \sqrt{g_*} x_F} \langle\sigma\beta\rangle_{T=T_F} \right] \quad (\text{B.3})$$

where  $g$  is the number of degrees of freedom of the DM species.

With hindsight, we know for weak multiplets the mass of the thermal relic will be of order a few TeV so we can neglect the effect of the mass splitting and consider the DM

multiplet as one species. In the annihilation cross-section calculation we also neglect the splitting and we consider all SM particles as massless. We expect  $x_F \sim 25$  so we will take the non-relativistic limit in the thermal average computation using the Maxwell-Boltzmann distribution:

$$f(\beta_{12}, x) = 4\pi \left(\frac{x}{4\pi}\right)^{\frac{3}{2}} \beta_{12}^2 \exp\left(-\frac{x\beta_{12}^2}{4}\right) \quad (\text{B.4})$$

The annihilation cross section is often expanded in the non-relativistic limit:  $\sigma\beta_{12} = a + b\beta_{12}^2 + O(\beta_{12}^4)$ . In this case, the thermal average can be computed explicitly and we get:

$$\int_{x_F}^{\infty} \frac{\langle\sigma\beta_{12}\rangle}{x^2} dx = \frac{1}{x_F} \left[ a + \frac{3b}{x_F} + O\left(\frac{1}{x_F^2}\right) \right] \quad (\text{B.5})$$

We also take into account the 1-loop SM running of the  $g_L$  and  $g_Y$  coupling constants and evaluate these at the scale  $M$ , corresponding to the approximate energy scale of the annihilation process in the nonrelativistic limit.

### B.1 Pure Higgsino

For the relic density calculation, we expect freeze-out to happen around  $x \sim 25$  and so we expect the velocity thermal distribution to peak around  $\beta_{12} \sim 0.4$ . For TeV-scale DM mass and splittings below a GeV, annihilation occurs comfortably above the threshold for on-shell production of the charged pair  $\text{DM}^+\text{DM}^-$ ,  $\beta_{12,\text{th}} \sim 5 \times 10^{-2}$ . In this regime we expect the potential due to the weak interaction to dominate over the hypercharge part, and can use the analytical computation of the Sommerfeld factor in the limit  $g_Y, \delta m \rightarrow 0$  to estimate the relic density.

In this simple limit, the potential matrix in the  $Q = 0$  sector can be diagonalized:

$$V_{Q=0}(r) = R \begin{pmatrix} \frac{1}{4} & 0 \\ 0 & -\frac{3}{4} \end{pmatrix} R^T \frac{\alpha_L}{r} e^{-M_W r} \quad \text{where} \quad R = \frac{1}{\sqrt{2}} \begin{pmatrix} 1 & 1 \\ -1 & 1 \end{pmatrix} \quad (\text{B.6})$$

yielding one attractive channel and one repulsive channel.

The attractive Yukawa channel has an effective coupling of  $\frac{3}{4}\alpha_L = 0.025$  so we expect a large Sommerfeld enhancement close to specific masses at which there is a bound state close to threshold (zero-energy bound state), similar to the thermal wino case. The first resonance is predicted by equation (1.16) to be at  $M = \frac{4kM_W}{3\alpha_L} = 5.25$  TeV, far above the Higgsino DM relic mass obtained from the perturbative calculation.<sup>7</sup>

Using these approximate formulas, we can compute the Higgsino relic density for different DM masses. The result is shown in figure 8; we see that Sommerfeld enhancement is completely negligible for a wide range of masses, even close to the resonant mass. Numerical calculations confirm that Sommerfeld enhancement has almost no effect on nominal Higgsino DM with  $\delta m = 344$  MeV, which remains unchanged at  $M = 1.1$  TeV.

For nominal splitting, the first resonance appear for a large Higgsino mass around 6.4 TeV, much above the perturbative relic mass result. But even on resonance, Sommerfeld enhancement is negligible in the relic density calculation. This can already be seen in the analytical result in figure 8, where the resonance is predicted at 5.3 TeV but is not visible

---

<sup>7</sup>The positions of the first resonance with non zero  $\delta m$  has to be computed numerically and is shown on figure 3 (left).

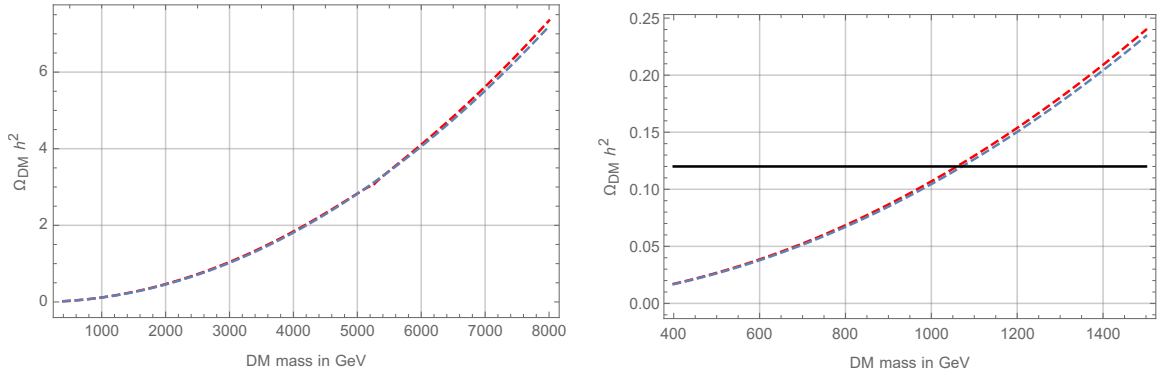


**Figure 8.** Relic density for a thermal Higgsino as a function of Higgsino mass. We show the standard tree-level perturbative result for the  $l = 0$  channel (blue dashed line), and the corresponding result including the non-perturbative effect computed using the analytical Sommerfeld factor in the  $g_Y, \delta m \rightarrow 0$  limit (red dashed line), as described in the text.

on the relic density curve. On resonance, we see a big increase in the annihilation cross-section at very low velocity but almost no Sommerfeld enhancement at velocities relevant at freeze-out.

When decreasing the Higgsino charged-neutral splitting  $\delta m$ , the resonant mass decreases, and the resonance gets sharper, as seen in figure 3. However, as hinted by the analytical approximation, numerical calculations show that the resonance does not affect the relic density significantly. The annihilation cross-section receives a large boost at low velocity but is almost unchanged at velocities relevant at  $x_F \sim 25$  leading to very little change in the thermal average  $\langle \sigma \beta_{12} \rangle$ . Thus we expect the Higgsino relic mass to be insensitive to the precise value of the mass splitting.

This will remain true provided the splitting is negligible in comparison with the thermal kinetic energy at freeze-out, and the zero-splitting analytical approximation holds, for  $x_F \sim 25$  and  $M = 1.1$  TeV this condition corresponds to  $\delta m \ll 20$  GeV. Further increasing  $\delta m$  would bring the threshold (1.17) and the electromagnetic resonances (2.7) near the peak of the dark matter velocity distribution, likely resulting in a larger enhancement of the cross-section. This scenario will require light new physics which is not taken into account in our simplified models, and we will not consider it any further.

## B.2 Pure Wino

As in the Higgsino case, at velocities relevant for the relic calculation we expect the  $SU(2)_L$  part of the potential to dominate, and we can make an analytical estimate of the Sommerfeld factors in the limit  $g_Y, \delta m \rightarrow 0$ .

In the  $Q = 0, S = 0$  sector the potential matrix can be diagonalized:

$$V_{Q=0}^{S=0}(r) = R \begin{pmatrix} 1 & 0 \\ 0 & -2 \end{pmatrix} R^T \frac{\alpha_L}{r} e^{-M_W r} \quad \text{where} \quad R = \frac{1}{\sqrt{3}} \begin{pmatrix} 1 & \sqrt{2} \\ -\sqrt{2} & 1 \end{pmatrix} \quad (\text{B.7})$$

resulting again in one attractive channel and one repulsive channel.

For all other channels diagonalization is not necessary, and we simply replace compute the Sommerfeld factor replacing the Yukawa potential by the Hulthén potential. We estimate

the resonant masses for which the Sommerfeld factors will grow large at low velocity using equation (1.16) for the attractive channels. In the  $S0Q0$  channel, the attractive Yukawa potential has an effective coupling  $2\alpha_L$  so the first resonance is predicted to be at  $M = \frac{km_W}{2\alpha_L} = 1.97$  TeV. In the  $Q1$  channel, equation (1.16) gives:  $M = 3.94$  TeV and in the  $S1Q0$  channel  $M = 5.81$  TeV. The first resonance in the  $S0Q0$  sector is close to the value of the Wino DM mass predicted by the perturbative calculation and is the most important for Wino DM phenomenology. The effects of a non-zero mass splitting are shown in figure 2; in the nominal case  $\delta m = 165$  MeV the resonance lies at  $M = 2.37$  TeV.

We can then compute the Wino relic density as function of the DM mass. The result is shown on 9, we see that, unlike in the Higgsino case, Sommerfeld enhancement has a significant effect on the Wino relic density, of order 40 %. The difference with the Higgsino scenario comes from two features of the Wino model. First in the diagonalization of the potential matrices, we see that the attractive channels have a larger effective coupling in the Wino case than in the Higgsino case resulting to overall larger Sommerfeld factors. Second, the off-diagonal terms in the annihilation matrices are negative for the Higgsino and positive for the Wino; in other words interferences between the charged and neutral channel are constructive for the Wino and destructive for the Higgsino. Moreover we see that the resonance, predicted around 2 TeV in the  $\delta m = 0$  limit, has a very small effect on the relic density. The analytical approximation of Sommerfeld enhancement predicts the Wino DM mass to be  $M = (2925 \pm 15)$  GeV to get the correct relic abundance.

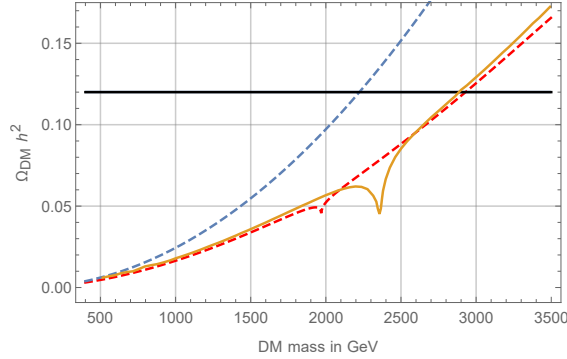


**Figure 9.** Relic density for thermal Wino DM as a function of Wino mass. We show the standard tree-level perturbative result for the  $l = 0$  channel (blue dashed line), and the corresponding result including the non-perturbative effect computed using the analytical Sommerfeld factor in the  $g_Y, \delta m \rightarrow 0$  limit (red dashed line), as described in the text. The solid orange line shows the numerical result extracted from [8], corrected to include the one-loop running of the gauge couplings.

The full numerical calculation for nominal splitting  $\delta m = 165$  MeV is well-approximated by the analytical result (see figure 9). In what follows we will take the Wino relic mass to be  $M = 2.9$  TeV.

The main discrepancy between numerical and analytical results happen around the resonance in the  $S0Q0$  sector. First, the position of the peak in the Sommerfeld enhancement is displaced from 1.97 TeV in the  $\delta m = 0$  limit to 2.37 TeV in the nominal splitting case. Furthermore, the dip caused by the resonance is more important in the full electroweak case than in the analytical prediction. We can see on figure 9 that the analytical formula underestimates the size of the Sommerfeld factors on resonance. At 2.9 TeV the two curves

agree very well and the resonance has negligible impact on the value of the Wino relic mass.

As for the Higgsino relic, the main effect of changing the Wino mass splitting is to shift the precise position of the resonance. This affects the Sommerfeld enhanced cross-section for small values of  $\beta$  but not the high values of  $\beta$  relevant for the relic density calculation. We see on figure 9 that the analytical curve is a very good approximation for the relic density outside of the resonance dip (around  $M = 2.37$  TeV) where the relic density is overestimated.

For a thermal Wino relic we are always in the regime  $\delta m \ll T_F$  so we expect the analytic prediction (matched by the numerical calculation for the nominal splitting  $\delta m = 165$  MeV) of  $M = 2.9$  TeV to be valid for all values of the mass splitting as long as the resonance is not located right at 2.9 TeV. This happens for  $\delta m = 450$  MeV; around this value we expect the relic mass to change by order a few hundred GeV. Again this will require light new states mixing with the Wino, and is outside the scope of this work.

## References

- [1] M. Battaglieri et al., *US Cosmic Visions: New Ideas in Dark Matter 2017: Community Report*, in *U.S. Cosmic Visions: New Ideas in Dark Matter College Park, MD, USA, March 23-25, 2017*, 2017. [arXiv:1707.04591](#).
- [2] M. Baryakhtar, J. Bramante, S. W. Li, T. Linden, and N. Raj, *Dark Kinetic Heating of Neutron Stars and An Infrared Window On WIMPs, SIMPs, and Pure Higgsinos*, *Phys. Rev. Lett.* **119** (2017), no. 13 131801, [[arXiv:1704.01577](#)].
- [3] R. Krall and M. Reece, *Last Electroweak WIMP Standing: Pseudo-Dirac Higgsino Status and Compact Stars as Future Probes*, *Chin. Phys.* **C42** (2018), no. 4 043105, [[arXiv:1705.04843](#)].
- [4] M. Low and L.-T. Wang, *Neutralino dark matter at 14 TeV and 100 TeV*, *JHEP* **08** (2014) 161, [[arXiv:1404.0682](#)].
- [5] R. Mahbubani, P. Schwaller, and J. Zurita, *Closing the window for compressed Dark Sectors with disappearing charged tracks*, *JHEP* **06** (2017) 119, [[arXiv:1703.05327](#)]. [Erratum: *JHEP*10,061(2017)].
- [6] A. Sommerfeld, *Über die beugung und bremsung der elektronen*, *Ann. Phys.* **11** (1931) 257.
- [7] J. Hisano, S. Matsumoto, M. M. Nojiri, and O. Saito, *Non-perturbative effect on dark matter annihilation and gamma ray signature from galactic center*, *Phys. Rev.* **D71** (2005) 063528, [[hep-ph/0412403](#)].
- [8] J. Hisano, S. Matsumoto, M. Nagai, O. Saito, and M. Senami, *Non-perturbative effect on thermal relic abundance of dark matter*, *Phys. Lett.* **B646** (2007) 34–38, [[hep-ph/0610249](#)].
- [9] N. Arkani-Hamed, D. P. Finkbeiner, T. R. Slatyer, and N. Weiner, *A Theory of Dark Matter*, *Phys. Rev.* **D79** (2009) 015014, [[arXiv:0810.0713](#)].
- [10] R. Iengo, *Sommerfeld enhancement: General results from field theory diagrams*, *JHEP* **05** (2009) 024, [[arXiv:0902.0688](#)].
- [11] M. Beneke, C. Hellmann, and P. Ruiz-Femenia, *Non-relativistic pair annihilation of nearly mass degenerate neutralinos and charginos III. Computation of the Sommerfeld enhancements*, *JHEP* **05** (2015) 115, [[arXiv:1411.6924](#)].
- [12] T. R. Slatyer, *The Sommerfeld enhancement for dark matter with an excited state*, *JCAP* **1002** (2010) 028, [[arXiv:0910.5713](#)].
- [13] A. Mitridate, M. Redi, J. Smirnov, and A. Strumia, *Cosmological Implications of Dark Matter Bound States*, *JCAP* **1705** (2017), no. 05 006, [[arXiv:1702.01141](#)].

- [14] S. Cassel, *Sommerfeld factor for arbitrary partial wave processes*, *J. Phys.* **G37** (2010) 105009, [[arXiv:0903.5307](#)].
- [15] M. Cirelli, P. Panci, K. Petraki, F. Sala, and M. Taoso, *Dark Matter’s secret liaisons: phenomenology of a dark  $U(1)$  sector with bound states*, *JCAP* **1705** (2017), no. 05 036, [[arXiv:1612.07295](#)].
- [16] P. Asadi, M. Baumgart, P. J. Fitzpatrick, E. Krupczak, and T. R. Slatyer, *Capture and Decay of Electroweak WIMPonium*, *JCAP* **1702** (2017), no. 02 005, [[arXiv:1610.07617](#)].
- [17] E. Braaten, E. Johnson, and H. Zhang, *Zero-range effective field theory for resonant wino dark matter. Part III. Annihilation effects*, *JHEP* **05** (2018) 062, [[arXiv:1712.07142](#)].
- [18] S. D. Thomas and J. D. Wells, *Phenomenology of Massive Vectorlike Doublet Leptons*, *Phys. Rev. Lett.* **81** (1998) 34–37, [[hep-ph/9804359](#)].
- [19] **XENON** Collaboration, E. Aprile et al., *Dark Matter Search Results from a One Ton-Year Exposure of XENON1T*, *Phys. Rev. Lett.* **121** (2018), no. 11 111302, [[arXiv:1805.12562](#)].
- [20] J. Bramante, P. J. Fox, G. D. Kribs, and A. Martin, *Inelastic frontier: Discovering dark matter at high recoil energy*, *Phys. Rev.* **D94** (2016), no. 11 115026, [[arXiv:1608.02662](#)].
- [21] M. Cirelli, N. Fornengo, and A. Strumia, *Minimal dark matter*, *Nucl. Phys.* **B753** (2006) 178–194, [[hep-ph/0512090](#)].
- [22] M. Cirelli, A. Strumia, and M. Tamburini, *Cosmology and Astrophysics of Minimal Dark Matter*, *Nucl. Phys.* **B787** (2007) 152–175, [[arXiv:0706.4071](#)].
- [23] T. Cohen, M. Lisanti, A. Pierce, and T. R. Slatyer, *Wino Dark Matter Under Siege*, *JCAP* **1310** (2013) 061, [[arXiv:1307.4082](#)].
- [24] J. Fan and M. Reece, *In Wino Veritas? Indirect Searches Shed Light on Neutralino Dark Matter*, *JHEP* **10** (2013) 124, [[arXiv:1307.4400](#)].
- [25] A. Bhattacharya and T. R. Slatyer, *Bound States of Pseudo-Dirac Dark Matter*, [[arXiv:1812.03169](#)].
- [26] G. Belanger, C. Boehm, M. Cirelli, J. Da Silva, and A. Pukhov, *PAMELA and FERMI-LAT limits on the neutralino-chargino mass degeneracy*, *JCAP* **1211** (2012) 028, [[arXiv:1208.5009](#)].
- [27] A. Cuoco, J. Heisig, M. Korsmeier, and M. Krmer, *Constraining heavy dark matter with cosmic-ray antiprotons*, *JCAP* **1804** (2018), no. 04 004, [[arXiv:1711.05274](#)].
- [28] **H.E.S.S.** Collaboration, H. Abdallah et al., *Search for dark matter annihilations towards the inner Galactic halo from 10 years of observations with H.E.S.S.*, *Phys. Rev. Lett.* **117** (2016), no. 11 111301, [[arXiv:1607.08142](#)].
- [29] **Fermi-LAT** Collaboration, M. Ackermann et al., *Searching for Dark Matter Annihilation from Milky Way Dwarf Spheroidal Galaxies with Six Years of Fermi Large Area Telescope Data*, *Phys. Rev. Lett.* **115** (2015), no. 23 231301, [[arXiv:1503.02641](#)].
- [30] K. Blum, R. Sato, and T. R. Slatyer, *Self-consistent Calculation of the Sommerfeld Enhancement*, *JCAP* **1606** (2016), no. 06 021, [[arXiv:1603.01383](#)].
- [31] M. Cirelli, T. Hambye, P. Panci, F. Sala, and M. Taoso, *Gamma ray tests of Minimal Dark Matter*, *JCAP* **1510** (2015), no. 10 026, [[arXiv:1507.05519](#)].
- [32] S. Kim and M. Laine, *On thermal corrections to near-threshold annihilation*, *JCAP* **1701** (2017) 013, [[arXiv:1609.00474](#)].
- [33] T. Binder, L. Covi, and K. Mukaida, *Dark Matter Sommerfeld-enhanced annihilation and Bound-state decay at finite temperature*, *Phys. Rev.* **D98** (2018), no. 11 115023, [[arXiv:1808.06472](#)].

- [34] S. P. Martin, *A Supersymmetry primer*, [hep-ph/9709356](#). [Adv. Ser. Direct. High Energy Phys.18,1(1998)].
- [35] E. J. Chun, J.-C. Park, and S. Scopel, *Non-perturbative Effect and PAMELA Limit on Electro-Weak Dark Matter*, *JCAP* **1212** (2012) 022, [[arXiv:1210.6104](#)].
- [36] G. Belanger, K. Benakli, M. Goodsell, C. Moura, and A. Pukhov, *Dark Matter with Dirac and Majorana Gaugino Masses*, *JCAP* **0908** (2009) 027, [[arXiv:0905.1043](#)].
- [37] **ATLAS** Collaboration, G. Aad et al., *Search for charginos nearly mass degenerate with the lightest neutralino based on a disappearing-track signature in pp collisions at  $\sqrt{s}=8\text{TeV}$  with the ATLAS detector*, *Phys. Rev.* **D88** (2013), no. 11 112006, [[arXiv:1310.3675](#)].
- [38] S. Nussinov, L.-T. Wang, and I. Yavin, *Capture of Inelastic Dark Matter in the Sun*, *JCAP* **0908** (2009) 037, [[arXiv:0905.1333](#)].
- [39] G. Servant and T. M. P. Tait, *Is the lightest Kaluza-Klein particle a viable dark matter candidate?*, *Nucl. Phys.* **B650** (2003) 391–419, [[hep-ph/0206071](#)].
- [40] **Particle Data Group** Collaboration, K. A. Olive et al., *Review of Particle Physics*, *Chin. Phys.* **C38** (2014) 090001.